David Gebhart , BSc

Production and Characterization of Screen-Printed Magnetoelectric Sensors

MASTER'S THESIS

to achieve the university degree of

Diplom-Ingenieur

Master's degree programme: Advanced Materials Science

submitted to

Graz University of Technology

Supervisor

Univ.-Prof.i.R. Dr.phil. Heinz Krenn

University of Graz

Institute of Physics

Graz, July 2020

AFFIDAVIT

I declare that I have authored this thesis independently, that I have not used other than the declared sources/resources, and that I have explicitly indicated all material which has been quoted either literally or by content from the sources used. The text document uploaded to TUGRAZonline is identical to the present master's thesis.

Date, Signature

Abstract

A ferromagnetic core with a variable air gap of 3 mm up to 30 mm allows the generation of steady state magnetic fields from 190 mT (gap = 30 mm) to 630 mT (5 mm) for continuous operation. The maximum achieved field intensity is 910 mT (gap = 3 mm) up to a duration of 1 minute. Superimposed to the DC field, a Helmholtz coil pair generates a frequency variable AC field of a maximum of 7 mT at 10 kHz, which serves as exciting field for a phase sensitive detection of the magnetoelectric effect in magnetic polymer foils.

Sensor prototypes of a magnetoelectric nanocomposite consisting of a copolymer of polyvinylidene fluoride and polytrifluoroethylene P(VDF/TrFE) and cobalt ferrite ($CoFe_2O_4$) nanoparticles were produced by screen printing. An alternative sensor concept using magnetic ionic liquids in a P(VDF/TrFE) polymer matrix did not reproduce measurable magnetoelectric effects as published in literature. While no magnetoelectric voltage coefficient could be extracted by direct magnetic excitation, magnetoacoustic coupling has been proven as an alternative concept to utilize mechanical resonances for magnetostrictive amplification of the magnetoelectric effect. The magnetoacoustic coupling is demonstrated using a laser vibrometer.

This thesis was written in cooperation with *Joanneum Research Forschungs GmbH* as part of an FFG-funded project on *Printed Ferroelectric and Multiferroic Nanocomposites for Selective Sensing*.

Contents

List of Figures

List of Abbreviations

ME ... magnetoelectric
P(VDF/TrFE) ... polyvinylidene fluoride and polytrifluoroethylene
CFO ... cobalt ferrite
MIL ... magnetic ionic liquid
bmim[$FeCl_4$] ... 1-butyl-3-methylimidazolium tetrachloroferrate
PEDOT:PSS ... poly(3,4-ethylenedioxythiophene) polystyrene sulfonate
GBL ... γ-butyrolactone
PET ... poly(ethylene terephthalate)
α ... magnetoelectric susceptibility
α^V ... magnetoelectric voltage coefficient
μ ... magnetic permeability
ϵ ... dielectric permittivity
B ... magnetic flux density
E ... electric field
P ... electric polarization
H ... magnetic field
t ... sample thickness
V ... voltage
S ... strain
k ,. coupling limiting coefficient in composites
α^M ... converse magnetoelectric coefficient
EMF ... electromotive force
PZT ... lead zirconium titanate
PVDF ... polyvinylidene fluoride
SEM ... scanning electron microscopy
FO ... magnetite
DMF ... N,N-dimethylformamide
FEMM ... Finite Element Method Magnetics
GUI ... graphics user interface
PET ... poly(ethylene terephthalate)

1 Introduction

The magnetoelectric (ME) effect describes the coupling of the electric and the magnetic polarization of a material. There is a wide variety of applications for ME materials, such as sensors, actuators, energy harvesting devices, memory storage, spintronics, or biomedical applications among others [1] [2] [3] [4] [5]. While there are some single-phase ME materials, they are rather scarce and extreme conditions are often needed to show a coupling of the two properties, or they generally show small coupling properties [6].

A lot of research focuses on material composites. Laminated bulk composites generally show good coupling properties, reaching coupling coefficients of around 10 V/(cm Oe) [7], with the downside of limitations in mechanical properties and durability. Composites of the piezoelectric polymer polyvinylidene fluoride with nanoparticles of magnetostrictive materials have gathered a lot of interest for improved mechanical properties and the possibility of cheap mass production [8]. An important industrial application of such nanocomposites could be in preventive maintenance in any kind of electromotor in production facilities. Cheaply mass produced magnetoelectric sensors could be put in various places within or around electric motors, sensing deviations from nominal values in magnetic field intensity, indicating a need for maintenance before a motor malfunctions and production has to be stopped.

Research indicates that a good way to create thin and flexible sensors is to have a combination of a 0-3 and a 2-2 composite [9], where magnetostrictive nanoparticles are incorporated into a layer of piezoelectric polymer with a second layer of the same piezoelectric polymer on top. This n-m notation for connectivity in ME composites denotes n dimensions the magnetostrictive phase expands into and the m dimension spread of the ferroelectric phase. 0 stands for dots, 1 for lines, 2 for layers, and 3 for bulk. A sketch of a 0-3, a 2-2, and a hybrid ME composite can be seen in Fig. 1.1.

An obstacle in the study of ME materials is the measurement of small magnetoelectric coupling coefficients. A common method of measurement is applying a varying magnetic field and measuring the output voltage with a lock-in amplifier. A composite material's magnetoelectric voltage coefficient varies with both the

frequency of the AC magnetic field and the intensity of an overlayed DC magnetic bias field. To properly characterize a magnetoelectric material, one has to simultaneously generate large DC magnetic fields and AC magnetic fields of frequencies and intensities not easily achievable with AC current sources commonly found in laboratories.

In ME measurements, AC magnetic fields used often reach frequencies of up to 100 kHz and amplitudes above 10 Oe, which induces large parasitic signals stemming from electromotive forces or possibly from eddy currents [10, p. 150]. Another problem is that the piezoelectric phase of thin film magnetoelectric sensors reacts very sensitive to vibrations. In sensor prototypes without optimized production parameters, the magnetoelectric coupling can be small and it can be difficult do discern the magnetoelectric signal from parasitic signals.

A very recent approach to magnetoelectric thin film sensors uses magnetic ionic liquids. Studies have shown a magnetoelectric coupling two orders of magnitude larger than that of comparable nanocomposite materials [11]. An important advantage of such sensors over magnetostriction based sensors is that they do not need a magnetic bias to operate at their maximum sensitivity.

The main goal of this work was to set up a testing environment for the direct magnetoelectric effect. A first prototype of flexible composite thin film magnetoelectric sensors were produced, with an emphasis on cheap production cost and an easy scale up process.

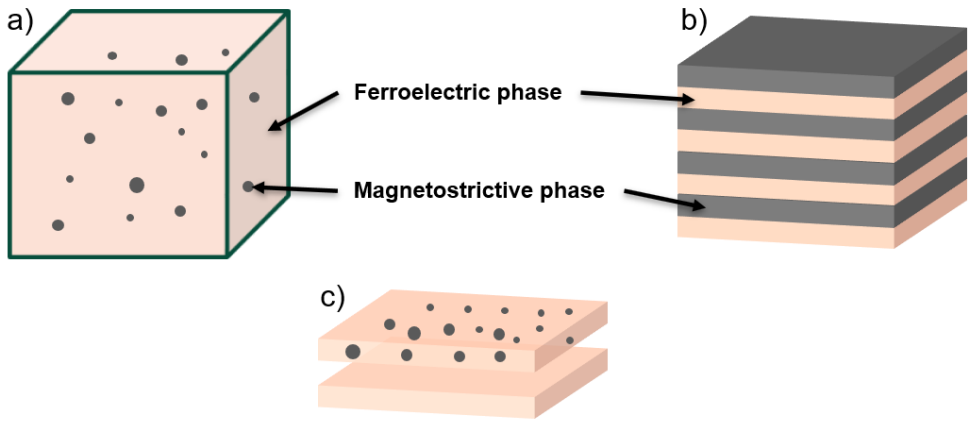

Figure 1.1: Sketch of a) a 0-3 connected composite, b) a 2-2 connected composite, and c) two layers of a hybrid 0-3 and 2-2 connected composite

2 Theory

2.1 Magnetoelectric Effect

The magnetoelectric effect is defined as a change in electric polarization of a material with an externally applied magnetic field, dP/dH (direct ME effect), or a change in magnetization with an applied electric field, dM/dE (converse ME effect).

As early as 1888, W. C. Röntgen investigated a magnetization of a spinning dielectric plate between two electrodes [12] and the term *magnetoelectric* was first used in 1926 by P. Debye [13] [2]. In the 1960s, studies were done on single-phase, or intrinsic, magnetoelectric materials, starting with the discovery of an electric polarization in cromium oxide (Cr_2O_3) by the application of an external magnetic field, first measured by D. N. Astrov [14] after being predicted by I. E. Dzyaloshinskii [15].

In intrinsic magnetoelectric materials, there is an upper bound of the magnetoelectric susceptibility for the system to be thermodynamically stable:

$$\alpha_{ij} < (\mu_{ii}\epsilon_{jj})^{\frac{1}{2}} \tag{2.1}$$

with magnetoelectric susceptibility α, magnetic permeability μ, and dielectric permittivity ϵ, all in the form of second rank tensor components [16] [6]. This upper bound poses a problem, as most intrinsic materials show either low dielectric permittivity or low magnetic permeability [17, p. 98]. Therefore a lot of research nowadays focuses on magnetoelectric composites, where this limit does not apply.

2.1.1 Magnetoelectric Composites

In magnetoelectric composites, the magnetoelectric effect stems from a coupling of magneto- and electrostrictive properties of its components, where the electrostrictive material is ferroelectric and it generally has to be electrically poled, applying large electric fields. Various studies have been done on composites of ferroelectric

and magnetostrictive ceramics, mostly using PZT as the piezoelectric phase and ferrites as the magnetostrictive phase. Such ceramic composites were mainly produced with 0-3 or 2-2 connectivity.

0-3 connected composites show a downside due to the poling process of the ferroelectric phase, where the sample has to be exposed to large electric fields and the lower electric resistivity of the magnetostrictive phase can lead to electrical breakdowns. Another problem are leakage currents, decreasing the composite's ability to store induced electric polarization [17, p. 117].

2-2 ceramic composites can be created by layer-by-layer growth, co-firing, or with an epoxy interlayer as laminates, with the latter showing the best reliability and reproduceability, and good strain coupling properties. A general downside to ceramic composites is their brittleness, making it hard to produce mechanically stable thin films. In sensor applications of the magnetoelectric effect, there is a need for low cost mass production of flexible sensors with high stability and a high degree of freedom in design.

Over the last decade a lot of studies have been done on composites using PVDF-based (polyvinylidene fluoride) polymers as the piezoelectric phase to achieve those desireable properties for magnetoelectric sensors. First approaches incorporated magnetostrictive nanoparticles into viscous solutions of PVDF, which were then spread out by doctor blades to form thin layers, sandwiched between two electrodes [18] [19] [20].

Such nanocomposites show similar problems as ceramic 0-3 composites. Dielectric breakdown can occur during the electrical poling of the ferroelectric phase if the content of the lower resistive magnetostrictive nanoparticles is too high, and leakage currents can lead to a dissipation of stored electric potential. The magnetoelectric coefficients were generally 2-3 orders of magnitude lower than in laminated ceramic composites [19] [7].

In 2019, A.C. Lima et al. [9] created a novel hybrid magnetoelectric composite with 0-3 as well as 2-2 connectivity. They dispersed cobalt ferrite ($CoFe_2O_4$) nanoparticles in a solution of a copolymer of polyvinylidene fluoride and polytrifluoroethylene P(VDF/TrFE). After applying a composite layer by doctor blade, they added a second layer of P(VDF/TrFE) between Ag electrodes on top. While they only poled the pure P(VDF/TrFE) layer, in this work we will show that it is possible to have both layers sandwiched between the electrodes, possibly further improving connectivity and additionally benefiting from the piezoelectric com-

ponent in the 0-3 connected composite. Lima's group was able to improve the magnetoelectric voltage coefficient to 164 mV/(cm Oe), from 11.2 mV/(cm Oe) of a 0-3 $CoFe_2O_4$/PVDF composite [20] [9]

2.1.2 Magnetoelectric Susceptibility and the magnetoelectric Voltage Coefficient

The magnetoelectric susceptibility is the fundamental magnetoelectric parameter, analogous to dielectric permittivity and magnetic permeability [21]. In an anisotropic material it has the form of a second rank tensor and has equal values for direct and converse magnetoelectric coupling [22]. It is given as

$$\alpha_{ij} = \frac{\partial B_i}{\partial E_j} = \frac{\partial P_i}{\partial H_j} \tag{2.2}$$

with magnetic flux density B, electric field E, electric polarization P, and magnetic field H. It is expressed in SI units as [s/m] [6].

Most research on the direct magnetoelectric effect focuses on the magnetoelectric voltage coefficient $\alpha_{ij}^V = \partial E_i / \partial H_j$. With E=V/t, it can be given as

$$\alpha_{ij}^V = \frac{1}{t}\frac{\partial V_i}{\partial H_j} \tag{2.3}$$

Using the relation $P_i = \epsilon_0 \chi_{ii} E_i \cong \epsilon_0 \epsilon_{ii} E_i$ for $\epsilon_{ii} \gg 1$, formula 2.2 can be rewritten as

$$\alpha_{ij} = \frac{\partial P_i}{\partial H_j} = \epsilon_0 \epsilon_{ii} \frac{\partial E_i}{\partial H_j} = \frac{\epsilon_0 \epsilon_{ii}}{t}\frac{\partial V_i}{\partial H_j} = \epsilon_0 \epsilon_{ii} \alpha_{ij}^V \tag{2.4}$$

with permittivity of vacuum ϵ_0, the material's relative permittivity ϵ, electric susceptibility χ, voltage V, and thickness t. In SI units the magnetoelectric voltage coefficient is expressed in [V/A], but in research it is almost always given in cgs units as [V/(cm Oe)].

An analogous expression for the magnetoelectric susceptibility in relation to the converse magnetoelectric coefficient ($\alpha_{ij}^M = \partial M_i / \partial E_j$) can be given as $\alpha_{ij} = \mu_0 \mu_{ii} \alpha_{ij}^M$.

2.2 The magnetoelectric Voltage Coefficient in Composites

In 2-phase composites, two distinct coupling properties, one in each phase, can generally lead to an overal composite coupling property, if both share one variable [23].

$$\begin{aligned} Material\ 1 &: \frac{dX}{dY} = a \\ Material\ 2 &: \frac{dY}{dZ} = b \\ Composite &: \frac{dX}{dZ} = abk \end{aligned} \tag{2.5}$$

with material variables X, Y, Z, coupling coefficients a, b, and a limiting coefficient k $\in$ [0,1). This limiting coefficient k stems from a different weighting of dY in the two materials due to limitations in coupling.

In ME composites, the direct magnetoelectric effect can be expressed as a product tensor property of two distinct phases, where one phase exhibits strain induced by a change in magnetic field (piezomagnetic coefficient), the other phase is strain coupled to the first one and exhibits electric polarization by the induced strain (piezoelectric coefficient). Together they can be thought of as a uniform material exhibiting an electric polarization, induced by a magnetic field (magnetoelectric effect). The magnetoelectric suceptibility can be given as

$$\alpha_{ij} = \frac{\partial P_i}{\partial S_{ij}} \frac{\partial S_{ij}}{\partial H_j} k \tag{2.6}$$

with electric polarization P, strain S, magnetic field H and a limiting coefficient k $\in$ [0,1). The limiting coefficient k is generally influenced by many factors, such as interface connectivity, interface area, and volume fractions of both components, among many others. It has to be noted that the piezoelectric coeffcient (the first fraction in 2.6) is a third rank tensor, but here the change of electric polarization with strain is reduced to a second rank tensor to keep the model simple.

Comparing 2.4 and 2.6, the magnetoelectric voltage coefficient can be given as

$$\alpha_{ij}^{V} = \frac{1}{t} \frac{\partial V_i}{\partial S_{ij}} \frac{\partial S_{ij}}{\partial H_j} k \tag{2.7}$$

with sample thickness t, and Voltage V.

Now this is a very simplified model, with most parameters hidden in k, but it shows three main routes of improving the voltage output of a magnetoelectric composite sensor:

i. $\partial V_i/\partial S_{ij}$ - choice of piezoelectric material

ii. $\partial S_{ij}/\partial H_j$ - choice of magnetostrictive material

iii. k - choice of interface connectivity and geometry

A lot of work on modeling the magnetoelectric effect in composites has been done by M. I. Bichurin and V. M. Petrov [24] [25] [26] [27], summarized and expanded on in a book released in 2014 [28].

2.3 Materials Selection

2.3.1 Piezoelectric Copolymer P(VDF/TrFE)

It was predetermined that this work should use a copolymer of vinylidene fluoride and trifluoroethylene, P(VDF/TrFE), as the piezoelectric phase. PVDF is a flexible ferroelectric polymer, considered as the best all-around electroactive material [29], reflected by an abundance of available literature on its use in magnetoelectric composites and an extensive in-house knowledge and research experience at *Joanneum Research - Materials*, manifested by a widely-used applicability as a flexible screen-printed sensor for pressure and temperature variations (PyzoFlex®).

PVDF is a semicrystalline material with a polymorphism of several crystalline phases. A sketch of three common phases can be seen in Fig. 2.1. The alpha phase has no permanent electric dipole moment, while beta and gamma phases exhibit paraelectric/ferroelectric behavior. Only the beta phase shows ferroelectric behaviour with a remnant electric polarization [30, p. xii].

The beta phase content of PVDF-based polymers can be increased by mechanical stretching, solidification under high pressure, or by poling under very large electric fields. With the addition of trifluoroethylene to vinylidene fluoride, the resulting copolymer's crystalline phase only shows β conformation, because is the only stable phase of the copolymer. Solidification from a solution in γ-butyrolactone (GBL) leads to high crystallinity in the polymer. For further reading on P(VDF/TrFE) solidified from a solution in GBL, a review article from Stadlober et al. [31], published in 2019, is recommended.

To activate the sensing capabilities of the polymer, the electric dipole moments have to be aligned by an electric field. Fig. 2.2 shows the observed current through

a reversal in polarization in the poling process of a P(VDF/TrFE) sample and the calculated electric displacement. At the bottom of the figure the rotation of a β-phase-molecule along its carbon backbone axis is illustrated, which happens at the coercive field (E_C). From the hysteresis curve, the remnant polarization of the sample can be taken, which is an important indicator for the quality of the sample and is in the range of 70 mC/m^2 for P(VDF/TrFE) copolymers [32].

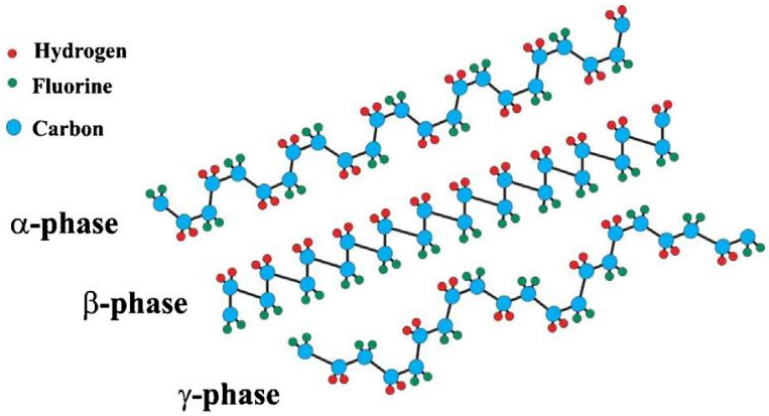

Figure 2.1: Chain conformation of α-, β-, and γ-phases of PVDF [29]

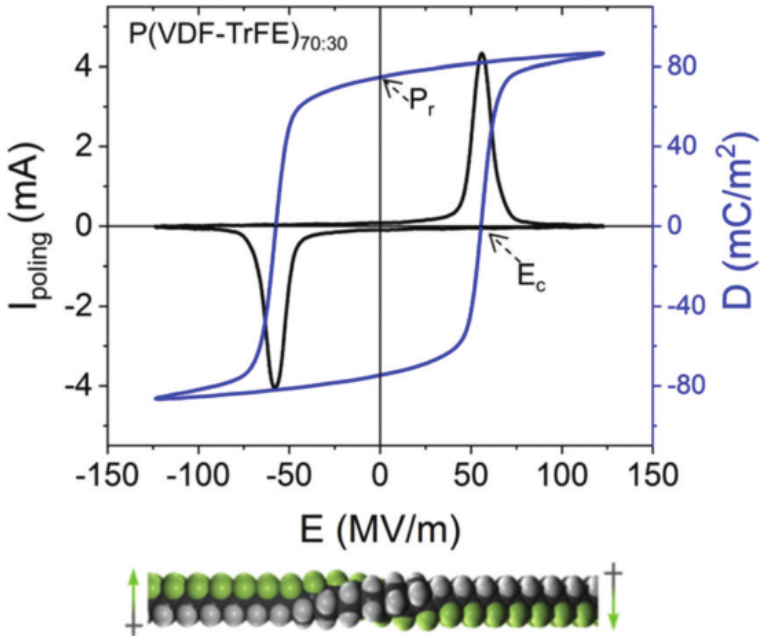

Figure 2.2: Measured switching currents and calculated electric displacement for a P(VDF/TrFE) copolymer sample during the poling process [31]

2.3.2 Magnetostrictive Material

The main approach taken in this work is to disperse magnetostrictive nanoparticles in a piezoelectric polymer solution, depositing that dispersion on a substrate and evaporating the solvent. Fig. 2.3 shows a homogenous distribution of magnetite (Fe_3O_4) nanoparticles in one of the samples produced within this work.

Since the nanoparticles are never magnetically poled and since they are randomly alligned in the composite, any anisotropy of magnetostriction is absent and the only magnetostrictive material property that has to be considered is joule magnetostriction.

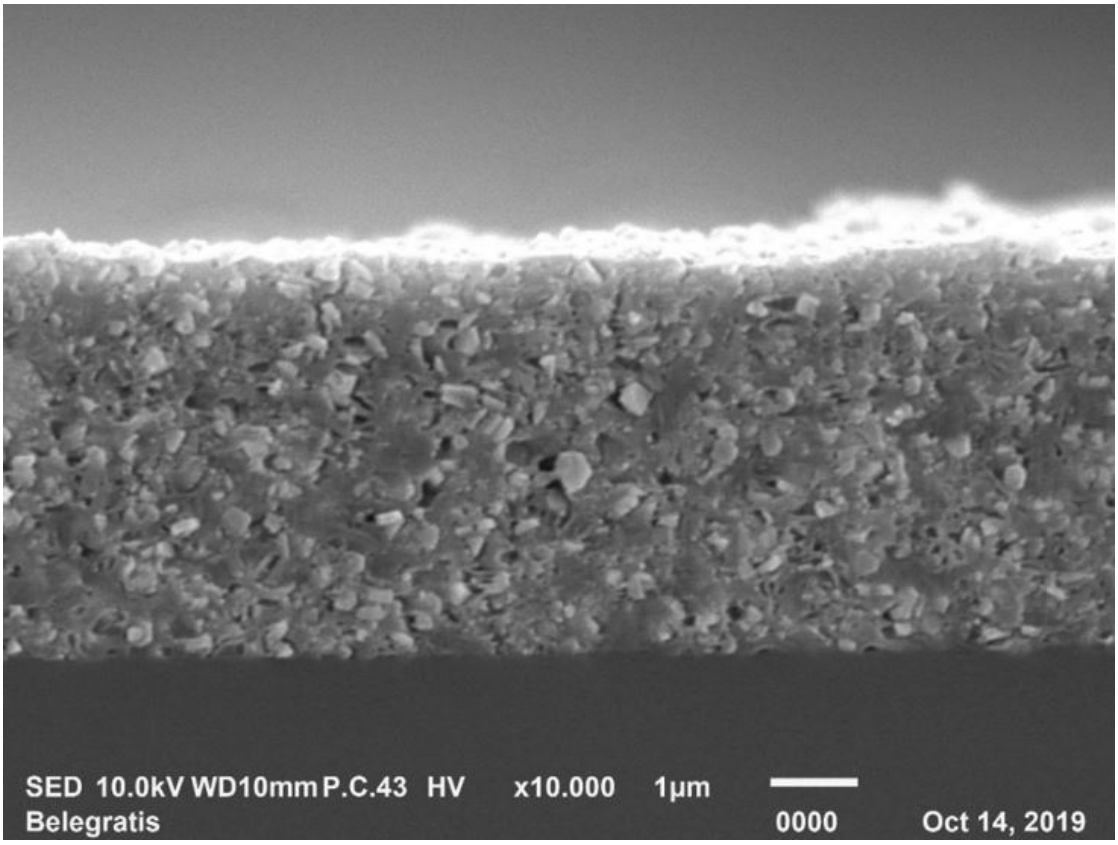

Figure 2.3: SEM image of a microtome cut of 50 wt% magnetite nanoparticles in P(VDF/TrFE) after solvent evaporation

By equation 2.7, the parameter to be optimized with the selection of a suitable magnetostrictive material is

$$\frac{\partial S_{ij}}{\partial H_j}$$

with Strain S and magnetic field H. As stated before, our sample is not expected to show intrinsic anisotropy and left with joule magnetostriction, $| \partial S_{ij}/\partial H_j |$ can be expected to show a maximum when i=j.

This property, dS/dH, is the definition of the piezomagnetic coefficient and there is broad consent in literature that the magentoelectric voltage coefficient is directly correlated to the piezomagnetic coefficient [17, p. 95] [28, p. ix] [10, p. 14]. The piezomagnetic coefficient is highly dependent on the applied magnetic bias field intensity and the goal is to find a material with a high peak in piezomagnetic coefficient at a relatively low magnetic field intensity. Ideally the piezomagnetic coefficient should show non-zero values at zero magnetic field, but in reality all known materials that can be used in such composites show very low piezomagnetic coefficients without an applied bias field.

In this work, cobalt ferrite ($CoFe_2O_4$; short: CFO) is chosen as a good candidate for the first patch of sensor prototypes. CFO shows one of the highest peaks in piezomagnetic coefficient in ceramics or polycrystalline alloys, with dS/dH in the range of 10^{-9} m/A, which peaks at a field intensity of around 100 kA/m for nanoparticle samples [33] [34].

In Fig. 2.4, the improved properties for magnetoelectric applications of CFO compared to Fe_3O_4 can be seen, with a magnetoelectric voltage coefficient almost one order of magnitude larger, as shown in ref. 8.

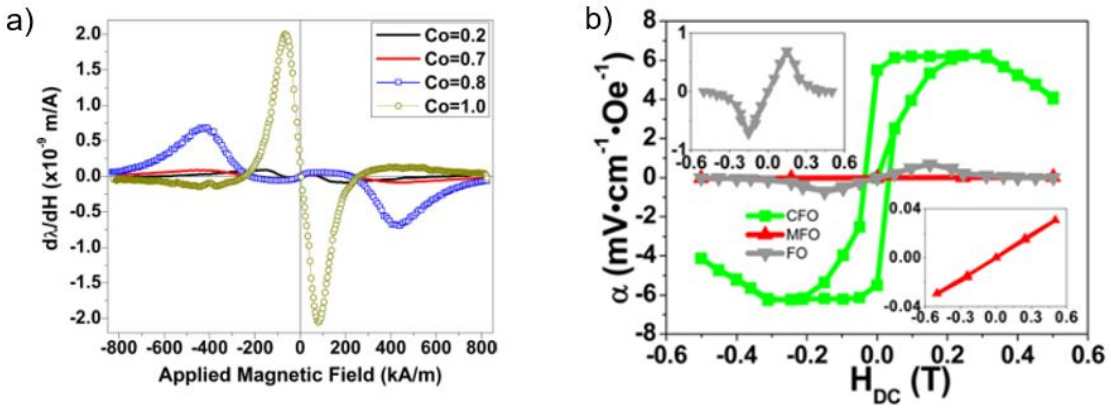

Figure 2.4: a) Increase in piezomagnetic coefficient with increasing cobalt content in $Co_xFe_{3-x}O_4$ [33] and b) comparision of magnetoelectric voltage coefficient of CFO, Fe_3O_4 (FO), and $Zn_{0.2}Mn_{0.8}Fe_2O_4$ (MFO) [8]

Some other materials are very promising for magnetoelectric applications, which will be discussed in the chapter *Outlook*.

2.4 Novel Approach using magnetic ionic Liquids

In 2018, D. Correia et al. [11] reported on a novel concept for magnetoelectric materials, using a magnetic ionic liquid (short: MIL), 1-butyl-3-methylimidazolium tetrachloroferrate (bmim[$FeCl_4$]), incorporated into a P(VDF/TrFE) matrix. The polymer matrix is non-active, only serving to encapsulate the MIL, making it a novel intrinsic magnetoelectric material. They were able to achieve a magnetoelectric voltage coefficient of 10 V/(cm Oe), two orders of magnitude larger than that of composites based on ferrites and P(VDF/TrFE).

Ionic liquids are defined as a salt with a melting point below 100 °C, with a subclass of room temperature ionic liquids (RTILs) often showing melting points below 0 °C. The reason for the low melting points are weak ionic interactions, which are explained by bulky ions, leading to larger distances between ionic charges, and delocalized electric charges within the ions themselves [36, p. 28] [37].

In MILs, one substituent of the ions has a net magnetic moment. In bmim[$FeCl_4$], the anion is a high-spin $[FeCl_4]^{-1}$-complex, which has a partially filled d-shell with 5 unpaired electrons. The anion's net magnetic moment is expected to be 5.9 μ_B, using $\mu_S = g(S(S+1))^{1/2}\mu_B$ with Landé g-factor g = 2, total spin quantum number S, and Bohr magneton μ_B [38, p. 169].

bmim[$FeCl_4$] is an oily liquid at RT, with a melting point of -8°C [39].

When a homogeneous magnetic field is applied to this MIL, the magnetic moments of the anions align and dipolar interactions lead to an ordering of the magnetic anions. Coupled with electrostatic forces, an ionic order can appear inside the liquid, leading to a macroscopic electric polarization of the MIL. If this MIL is brought between two electrodes and electrically isolated from them, a potential difference can be expected between those electrodes when a magnetic field is applied.

Correia et al. [11] have mixed bmim[$FeCl_4$] with a solution of P(VDF/TrFE) in N,N-dimethylformamide (DMF), spread it on a glass substrate and evaporated the solvent at 210 °C. The result was a porous polymer film with pockets of encapsulated MIL (Fig. 2.5). They then coated this film with Au electrodes on both sides, applied an AC magnetic field and measured the voltage difference of the two electrodes. Fig. 2.6 shows the voltage output of their samples as a function of frequency of an applied AC magnetic field of 2 Oe. At low frequencies a steep rise in voltage output can be observed, which flattens early on and then shows a peak somewhere between 10 and 20 kHz and starts to decrease again. As the paper states, this decrease shows that at higher frequencies time becomes the limiting

factor in the induced ionic ordering. That work does not address the steep rise in voltage output at very low frequencies, which might be an indication that the induced electric polarization is quenched by the timely electric-field induced cation movement.

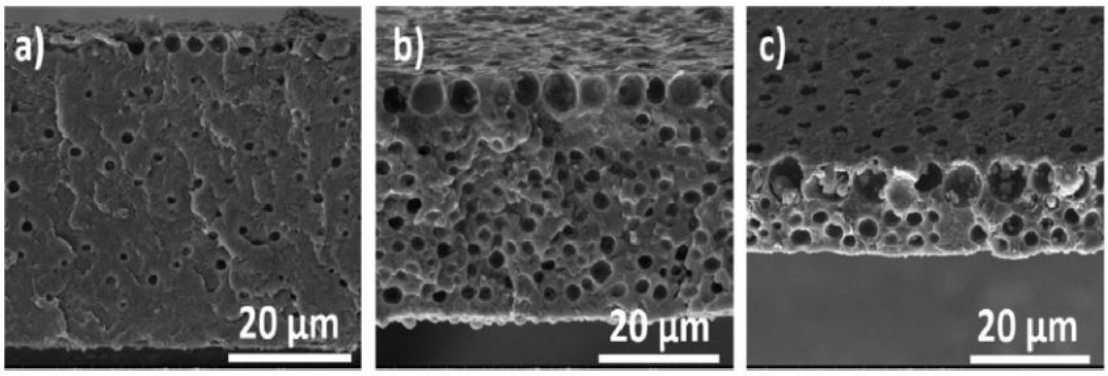

Figure 2.5: SEM images showing encapsulated MIL in polymer matrix. a) 10 b) 20 and c) 40 wt% [11]

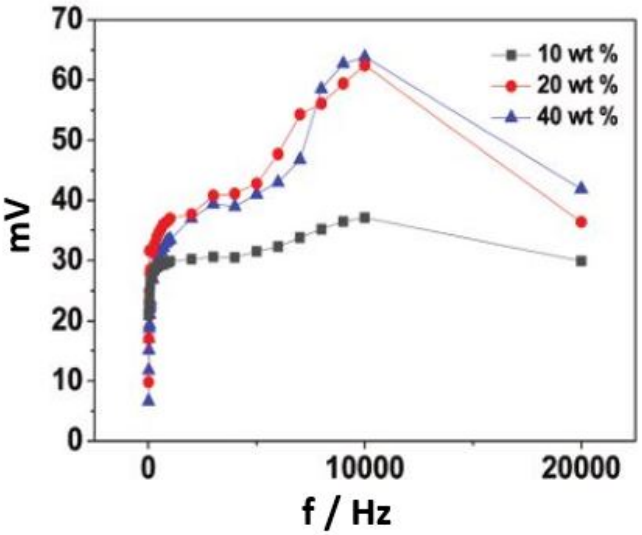

Figure 2.6: Frequency response of the voltage of a MIL composite for an AC magnetic field of 2 Oe [11]

3 Experimental Part

3.1 Test Bench

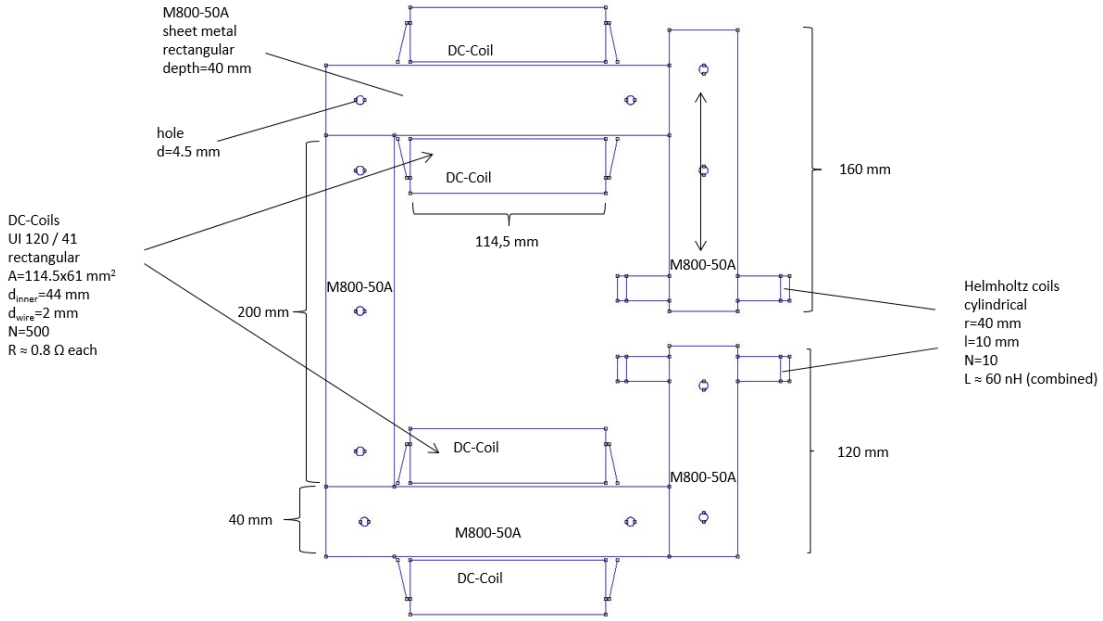

Figure 3.1: Sketch of the test bench

3.1.1 Setup

List of materials, components and electronic devices:

i. sheet metal M800-50A (Gebr. Waasner GmbH)

ii. coil bobbin UI 120/40 oD1 (Erwin Reumüller TEWA Elektromotorengesellschaft m.b.H.)

iii. 3D printed coil bobbin and core attachment (material VeroBlackPlus manufactured by Stratasys Ltd.)

iv. Signal Recovery 7265 DSP lock-in amplifier

v. Hubert A1110-16-QE 4-quadrant voltage and current amplifier

vi. TDK-Lambda GEN 30-50 power supply

vii. Agillent 81150A arbitrary waveform generator

viii. Fairchild Stealth Diode FFH50US60S

ix. NI GPIB-USB-HS

Two coils (ii) with 520 windings each, intended for dc operation, were produced by *Spalt Elektromechanik und Maschinenbau GmbH* using enameled copper wire (d=2 mm) on a coil bobbin of 12 cm length. To build up the magnetic core, the sheet metal (i) consists of a laminated stack with variable interlace, while being incorporated into the DC coils until a height of 40 mm was reached. This gives the magnetic core a cross section of 40 x 40 mm^2, with entire outer dimensions of 240 mm x 280 mm.

The core was tightened and fastened in place with brass screws on *item* aluminum profiles fixed on a wooden board. The aluminum profiles themselves were fixed with nonmagnetic screws. The DC coils were connected to the power supply (vi) in parallel. An FFH50US60S suppressor diode in forward direction connects the coils' output with their input to dissipate inductive voltage spikes when the supply current is reduced or switched off.

Two Helmholtz coils (iii) intended for AC operation were made by hand with 10 windings each of enameled copper wire (d=1 mm) on a 3D printed bobbin. The Helmholtz set-up has a radius of 40 mm and the coils are driven by a 4-quadrant amplifier (v), connected by two audio cables. The coils' bobbin can slide onto the magnetic core, placing one coil on each side of the air gap. The seonsors are then positioned inside the air gap using a non-magnetic mounting device, fixed at the edge of the table, to machanically decouple the samples from vibrations of the test bench core metal.

For the remote operation of the test bench the power supply is connected to a computer via a serial RS232 interface, while the lock-in amplifier (iv) and the function generator (vii) are controlled by GPIB using a GPIB to USB adapter (ix). The AC 4-quadrant amplifier is connected via USB.

After completion, the magnetic field intensities inside the electromagnet's gap and in the center of the AC coil were measured with an *F.W. Bell 7010 Gauss/Tesla Meter*. Measurements were done for various DC and AC current intensities and for different gap lengths.

3.1.2 Simulation

To estimate the magnetic field within the gap, simulations were done with *Finite Element Method Magnetics* (FEMM) 4.2, an open source software package, among other things, able to solve for 2D magnetic field patterns in AC or DC operation. The calculations were performed with an open boundary approximation, in which the software creates seven layers of Dirichlet boundary conditions. Meshes were generated automatically by the software.

Using Maxwell's equations and vector potentials, the software solves

$$\nabla \times (\frac{1}{\mu(B)} \nabla \times A) = J$$

for magnetostatic problems, with magnetic permeability μ, flux density B, vector potential A and current density J. For harmonic problems it decomposes to

$$\nabla \times (\frac{1}{\mu(B)} \nabla \times a) = -j\omega\sigma a + \hat{J}_{src} - \sigma \nabla V$$

with the complex number a stemming from a phasor transformation of A, electric conductivity σ, $\hat{J}_{src}$ is the phasor transform of the applied current sources, and voltage V.

Derivations and a more thorough explanation of the mathematics behind the software can be found in FEMM's manual [40].

3.2 Remote Control

An application for controlling the measurements and for data acquisition was implemented in Python 3.7. The package *PyQt5* 5.12 was used for the design and for the functionality of the graphics user interface (GUI). This package contains a *Qt Designer* application which was used to design the GUI and create a *.ui-file (XML format) that was then converted to python code by *pyuic5*, a *PyQt5* utility. The packages *pySerial* 3.4 and *PyVISA* 1.10 are used for serial and GPIB communication. Additional packages for the functionality of the GUI are *pandas, NumPy, ctypes, os*, and *time*.

The measurement parameters controlled by the remote operation are DC current, AC current amplitude, and frequency. Besides single measurements, three automated measurement functions are implemented: DC current sweeps at fixed frequencies, frequency sweeps at fixed DC Current intensities, and a fully automatic measurement, where both the frequency and the DC current are sweeped.

Data points are acquired for each parameter choice. The application waits until the lock-in amplifier has been locked to the reference signal, then four measurements of the lock-in's x-value are taken with a pause of 0.3 seconds between measurements. If the average of the first two and that of the second two measurements don't differ by more than 0.5 %, the average of all four values is stored and two measurements of all other values (y, magnitude and phase) are taken and each average is stored.

Data is stored over multiple measurements and can be exported as a *.csv file and deleted when convenient.

3.3 Ink Fabrication

3.3.1 Cobalt based Approach

Cobalt ferrite ($CoFe_2O_4$) (CFO) nanoparticles produced by Fraunhofer ISC were used as a magnetostrictive material, while a copolymer of PVDF (75%) and TrFE (25%) serves as the ferroelectric component in the sensors. The polymer was used in the form of a solution of 16 wt% P(VDF/TrFE) in γ-butyrolactone (GBL) (Piezotech FC25 INK GBL OP PIL 18/034 produced by Arkema S.A.).

For the magnetostrictive ink, a homogenous suspension of an equal amount of CFO and the dry mass of P(VDF/TrFE) in GBL was produced by adding 6.40 g of CFO to 40.0 g of the Piezotech solution in a 250 ml ZrO_2 ball mill container

along with 370 g of ZrO_2 balls (d=3 mm), both produced by Retsch GmBH. Another 18 ml of GBL were added to decrease the viscosity of the final suspension.

The mixture was milled in a Retsch PM 100 planetary ball mill at 500 rpm for 14 hours with a repeating interval of milling for one minute followed by a 2 minute break. The homogenous suspension was then separated from the ZrO_2 balls.

3.3.2 Magnetic ionic Liquid based Approach

A magnetic ionic liquid (MIL), 1-butyl-3-methylimidazolium tetrachloroferrate ([bmim][$FeCl_4$]), was obtained from *abcr GmbH*. Two magnetic ionic inks for screen printing were produced. One by combining 40.2 g *Piezotech* polymer solution (see above) with 0.35 g [bmim][$FeCl_4$] ($\equiv$ 5.2 wt% MIL after solvent evaporation) and another consisting of 41.0 g polymer solution and 2.09 g [bmim][$FeCl_4$] ($\equiv$ 24.2 wt% MIL after solvent evaporation). Each mixture was stirred with a glass rod for approximately one minute.

3.4 Sensor Design and Fabrication

The CFO based sensors are built-up of screen printed layers on a PET substrate, with poly(3,4-ethylenedioxythiophene) polystyrene sulfonate (PEDOT:PSS), serving as a screen-printable electrode material. The sensors characterized in this work consist of an electrode layer, a magnetostrictive composite layer, two layers of ferroelectric copolymer (*Piezotech*) and another electrode layer. A sketch is shown in Fig. 3.2.

The MIL based sensors are built up by a composite ink layer sandwiched between two *Piezotech* layers, with all three layers between two PEDOT:PSS electrodes. It should be noted that here the ferroelectric material just serves as a polymer matrix for the MIL and for electric isolation.

Finally, silver ink lines contacting the electrode layers were printed on top. After each printing process of a layer, the solvent was evaporated in an oven at 110 °C for 10 to 15 minutes.

Multiple sensor layouts were designed, with most of them designed with emphasis on compensation measurements. Two such sensors can be seen in Fig. 3.3. Sensor *Rfs* has a symmetrically split top electrode with the magnetostrictive phase spanning the whole active area. This way the ferroelectric layer can be poled in different directions on each half, giving the parasitic piezoelectric signals of the

two halves a phase difference of 180°. Another design (*Rhs*) also has a symmetrically split top electrode, with the magnetostrictive layer printed only on one half of the active area. With both halves poled in the same direction, the difference in their signals should be the magnetoelectric signal. After suspecting a transfer of bending vibrations from one side of the sensor to the other, most measurements were done by cutting an *Rhs* sensor design in the middle and taking measurements for each half individually.

The poling of the ferroelectric components of the CFO sensors was done by triangular waveform voltage of approximately 1.5 times the switching-current-peak voltage in both directions, with a frequency of 1 Hz over 20 periods. This poling process was performed 3 times for each sensor. For sensors with two ferroelectric layers, as depicted in Fig. 3.2, the applied voltage was ±1300 Volts.

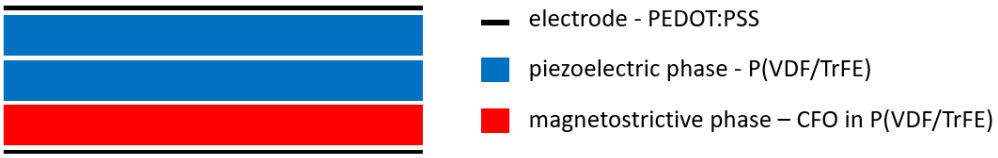

Figure 3.2: Sensor - layered set-up

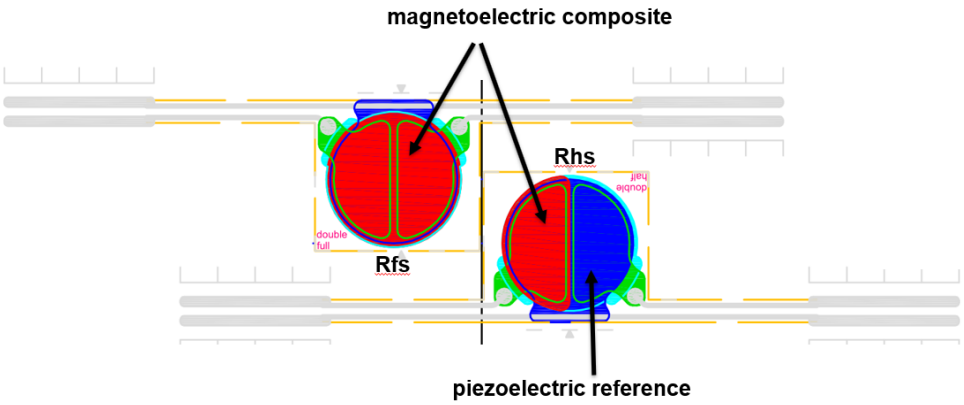

Figure 3.3: Sensor designs for compensation measurements

3.5 Measurement of the Magnetoelectric Voltage Coefficient

3.5.1 General Measurement Principle

There are a variety of measurement techniques for magnetoelectric coefficients, very well summarized in a review paper by M. M. Vopson et al [6]. This work uses a widely accepted method of measuring the magnetoelectric voltage coefficient by application of a DC bias magnetic field as well as a superimposed AC magnetic field and phase-synchronous (lock-in) measurement of the AC voltage response.

By integration of equation 2.3, the measured output voltage is given as

$$V_i = \alpha_{ij}^V t H_j \tag{3.1}$$

with voltage V, magnetoelectric voltage coefficient α_{ij}^V, sample thickness t and magnetic field H. The magnetic field H in this equation is the amplitude of the superimposed AC magnetic field.

As per equation 2.7, α^V (tensor notation will be omitted from here on out) is linearly dependent on the piezomagnetic coefficient dS/dH, which is generally not constant over the entire range of H, but can be approximated as constant over any sufficiently small interval.

Fig. 3.4 shows a simplified illustration of a static DC bias field (marked grey) with an intensity such that the slope of S is at its maximum within the interval of the dynamic AC magnetic field (marked red). At this point, α^V is at its maximum and therefore the measured output voltage also shows a maximum. The slope of the strain with respect to the magnetic field is the piezomagnetic coefficient dS/dH. Fig. 3.5 illustrates the general relation of strain (marked λ), piezomagnetic coefficient (marked q), and magnetoelectric voltage coefficient (marked α_{ME}) as a function of DC magnetic bias field.

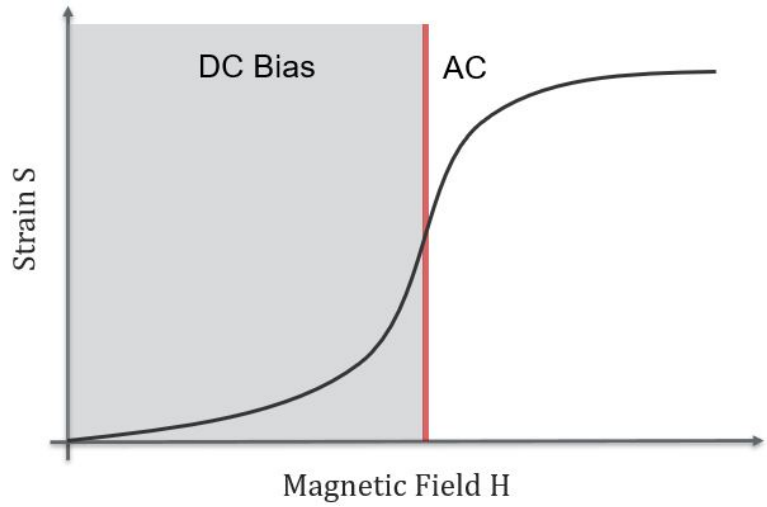

Figure 3.4: General illustration of the influence of DC field intensity on the measured slope with AC field modulation (red bar)

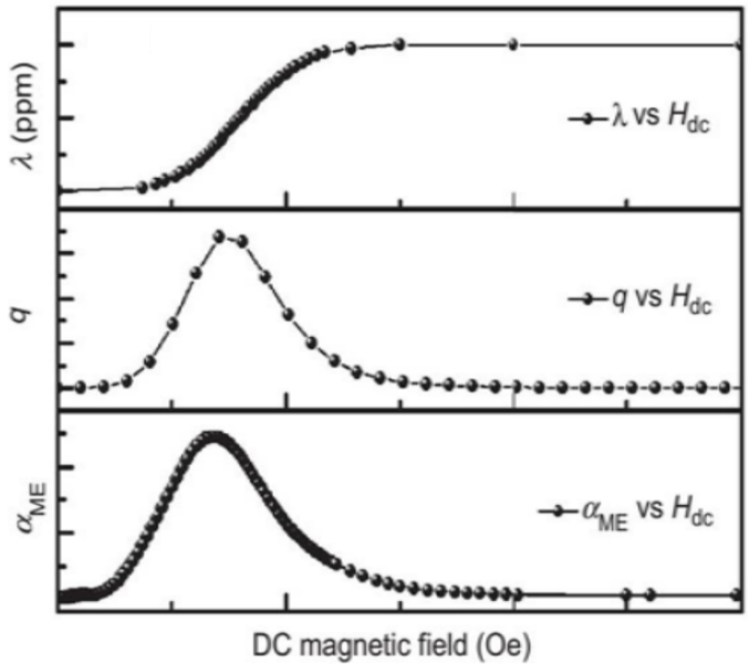

Figure 3.5: Relation of strain λ, piezomagnetic coefficient q, and magnetoelectric voltage coefficient α_{ME} [5]

3.5.2 Longitudinal and transversal Measurements

In 2-2 connected thin film magnetoelectric composites there are two ways of measuring the magnetoelectric voltage coefficient. With the composite film sandwiched between two electrodes, the electric polarization of the piezoelectric phase is always in the out-of-plane direction. In measurements of the direct magnetoelectric effect, the magnetostrictive phase can be magnetized in the in-plane direction, transversally to the electric polarization, or in the out-of-plane direction, longitudinally to the electric polarization (Fig. 3.6 a and b respectively). The notation of longitudinal and transversal is not consistent in literature and it is better to talk about in-plane and out-of-plane orientations.

Figure 3.6: a) Transversal or in-plane and b) longitudinal or out-of-plane orientation of the magnetization M

In a 2-2 connected magnetoelectric composite, two factors have to be considered that lead to differences in in-plane and out-of-plane measurements. First, assuming joule magnetostriction in the magnetostrictive phase, the expansive strain along the sample plane with in-plane magnetization should be approximately twice as large as a compressive strain in the sample plane direction with out of plane magnetization ($S_{\parallel} \approx -2\ S_{\perp}$) [35, p. 19]. Since only the strain within the sample plane can lead to strain coupling of the two layers, a larger magnetoelectric voltage output is expected with in-plane magnetization orientation.

The second factor to be considered is the demagnetizing field generated within the magnetostrictive phase. While no general magnetostrictive anisotropy can be expected for a bulk nanocomposite of magnetically randomly aligned nanoparticles, in thin films of high concentrations of magnetic nanoparticles, a macroscopic magnetic anisotropy may occur. When the concentration of nanoparticles is high enough, those nanoparticles could form clusters and should be in contact with each other at some points, or very close to each other at others (see Fig. 2.3).

This may lead to a decrease in the demagnetizing field in comparison to perfectly dispersed nanoparticles. The larger the length of the sample in the direction of magnetization, the more particles can be expected to be in contact with each other along that direction, therefore leading to easier magnetization within the film of the magnetostrictive phase in the direction of its plane. Fig. 3.7 shows a simplified illustration of this reduction of demagnetizing field (red arrow) with magnetization in the direction of the sample plane (yellow arrow).

This long-range anisotropy in magnetization could have the effect that the peak of the piezomagnetic coefficient shifts to higher magnetic field values for out-of-plane orientation. In out-of-plane measurements of the magnetoelectric voltage coefficient, its peak would also be found at higher DC bias fields compared to in-plane measurements of the same sample.

Fig. 3.8 can be interpreted to support the two assumptions mentioned above, with an overall decrease in α^V and a shift of its peak to larger bias fields in out-of-plane measurements [9].

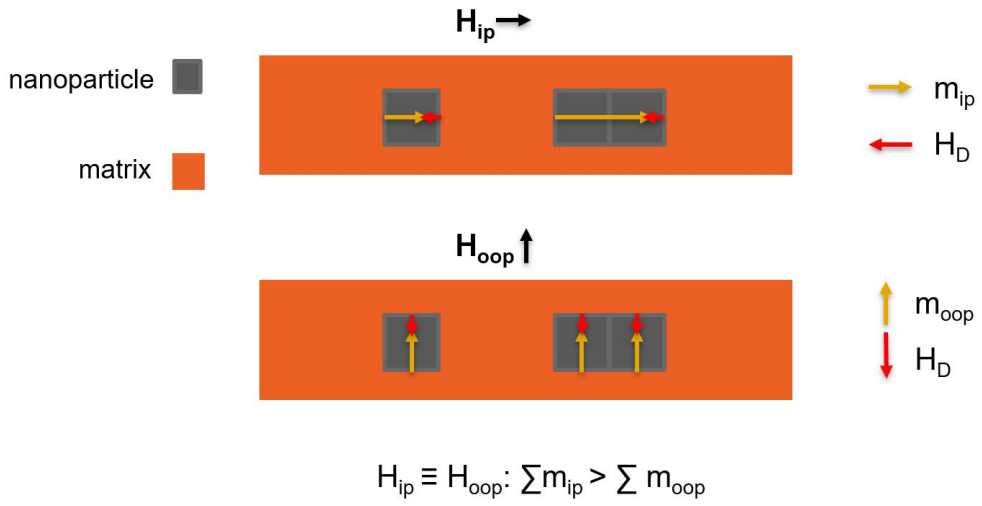

Figure 3.7: The in-plane magnetic moments m_{ip} are less reduced by the demagnetizing field H_D than the out-of-plane magnetic moments m_{oop}

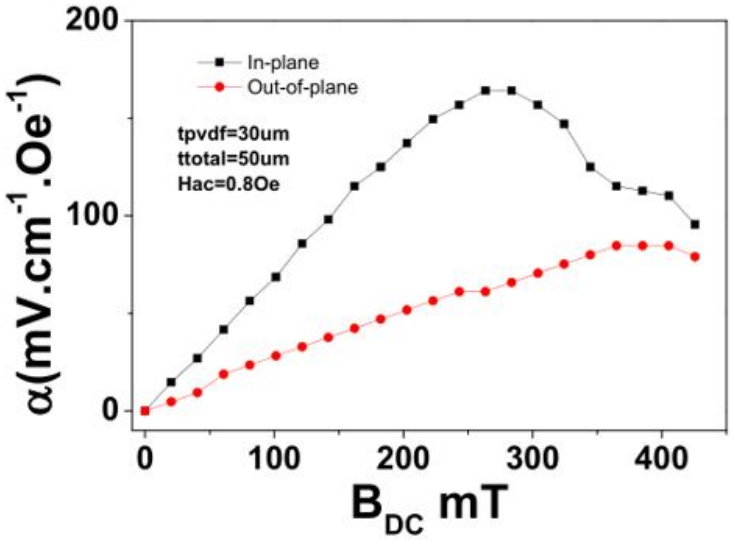

Figure 3.8: Comparision of in-plane (black) and out-of-plane (red) magnetoelectric voltage coefficient as a function of DC magnetic field for a 0-3 and 2-2 hybrid magnetoelectric composite of CFO and P(VDF/TrFE) [9]

3.5.3 Low Frequency Magnetic Field Effects in Composites

In measurements of the magnetoelectric voltage coefficient the frequency response of α^V has to be considered. Starting in the sub-Hz-region and up to around 10 kHz, 0-3 composites can show variations of α^V due to the Maxwell-Wagner effect (Fig. 3.9). A difference of dielectric permittivity of the piezoelectric and the magnetostrictive phases leads to frequency dependent interface coupling effects, influencing the bulk dielectric permittivity of the sample, the piezoelectric coefficient, and the magnetoelectric voltage coefficient. This effect induces a phase shift of measured output voltages [28, Chapter 3].

Studies of the magnetoelectric voltage coefficient of thin film composites generally show a single broad resonance frequency in the range of 10 kHz to 100 kHz, increasing the output voltage by approximately one order of magnitude (Fig. 3.10). Bichurin and Petrov have modeled several resonances for magnetoelectric composites up to frequencies of 10 GHz due to magneto-acoustig coupling [28]. The lowest electromechanical resonance frequencies arise from bending modes, which generally decrease with increasing sample length and with decreasing sample thickness. This fact is the reasoning that the lowest resonance frequency for a thin film magnetoelectric sample is the first bending mode.

The test bench set up in the scope of this work is designed to measure the di-

rect magnetoelectric effect up to a frequency of 100 kHz. Resonances other than bending modes are likely to occur at frequencies out of range of our measurements.

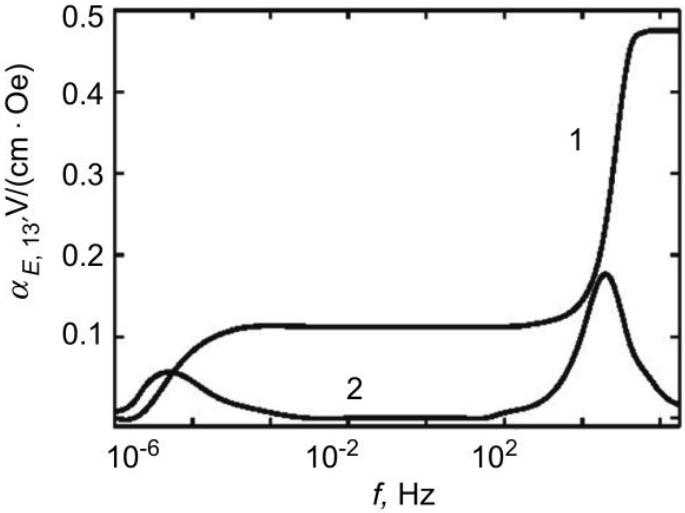

Figure 3.9: Modeled frequency dependance of real(1) and imaginary(2) parts of the magnetoelectric voltage coefficient in a ferrite-piezoelectric 0-3 composite [28, p. 54]

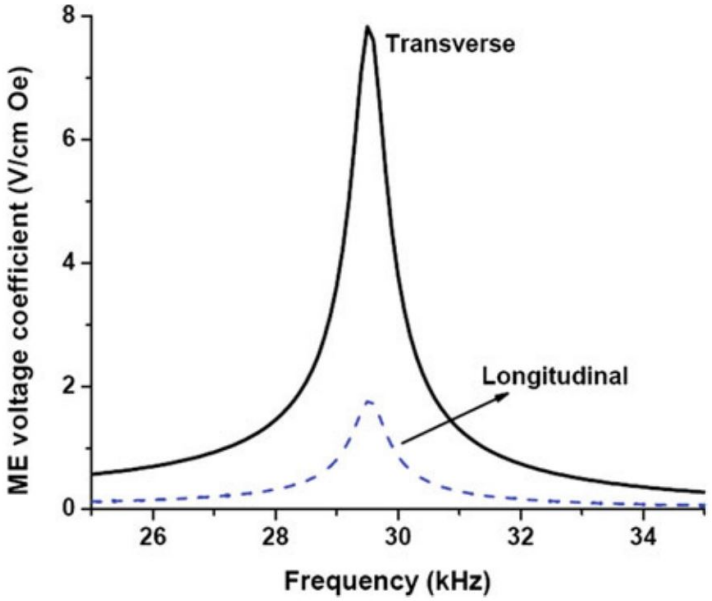

Figure 3.10: Modeled bending mode resonance in an unclamped bilayer of permendur and PZT of 9.2 mm length and 0.7 mm thickness [28, p. 68]

3.5.4 Obstacles in Measurements

It is generally not a trivial task to measure magnetoelectric voltages in thin film composites. The signals are rather small, overwhelmed by a variety of parasitic signals like signals from electromotive forces (EMF) or vibrations.

For optimized thin film ferrite-polymer composites driven at acoustic resonance, the magnetoelectric voltage coefficients are in the order of 100 mV/(cm Oe) [9]. The samples produced in this work have a thickness of around 20 μm and the maximum AC magnetic field intensity is around 120 Oe peak-to-peak. Assuming an achievable value of 100 mV/(cm Oe) for α^V and taking into account all other parameters of equation 3.1, the expected voltage output at resonance would be around 24 $\mathrm{mV_{PP}}$, or around 8 $\mathrm{mV_{rms}}$, with an approximately one order lower magnitude for out-of-resonance frequencies.

The measurement of such voltage signals is an easy task with lock-in amplifiers, but there are various parasitic signals that have to be suppressed in order to extract the magnetoelectric signal. Even with electromagnetically shielded connectors and optimized sensor design, small conducting loops and conducting electrode layers are sensitive antennas for picking up parasitic EMFs in the region of varying magnetic fields.

EMF signals may be discerned from ME signals in several ways. EMF voltage should increase linearly with frequency, while in non-resonant acoustic regions ME voltage should only exhibit slight and non-linear variations arising from Maxwell-Wagner effects (see 3.5.3). ME signals should possess either the same or the opposite phase with respect to the AC magnetic field, while signals arising from EMFs are 90° out-of-phase. Another method of discerning the two signals is a sweep of the DC bias field intensity. As mentioned earlier, the magnetoelectric voltage depends on the strain derivative (dS/dH), which greatly varies with bias field intensity, while EMF voltage should be independent of the DC bias field [10, p. 150].

Another problem are vibrations in the measurement set-up. If an AC field is applied inside the air gap of a DC electromagnet, it can permeate the magnetic core of the electromagnet, leading to vibrations through magnetostriction of the magnetic core material. Piezoelectric materials are quite sensitive to vibrations and if a measured ME composite sample is mechanically coupled to the DC core, those vibrations can lead to large parasitic signals in the piezoelectric response of the composite.

3.5.5 Conduction of Measurements

All signal carrying cables were electrically shielded. The function generator output was connected to the current amplifier, with a reference signal connected to the lock-in amplifier. The measured sample's top and bottom electrodes were connected to the lock-in amplifier's input channel. The samples were placed inside the air gap of the test bench with in-plane or out-of-plane field orientation with a flexible mount, not mechanically connected to the test bench itself.

To be able to get results without any influence from parasitic signals from electromotive forces, a *Polytec PDV-100 laser vibrometer* was used to determine magnetically induced vibrations of a composite sample. At mechanical resonance frequencies, a magnetoelectric composite sample and a piezoelectric reference sample were first excited by an AC voltage, and subsequently by an AC magnetic field, intending to induce vibrations by electrostriction and magnetostriction, respectively. The laser vibrometer's signal was acquired by a connection of its analog output to the lock-in amplifier.

4 Results

4.1 Test Bench

The measurement set-up can be seen in Fig. 4.1. A bendable nonmagnetic mount is used to place the samples inside the air gap. A connector to the lock-in amplifier is attached to the mount, where our printed sensors can simply be plugged in for measurements. First, a 3D printed attachment was used to mount the samples directly onto the magnetic core of the test bench, but there were problems with a transfer of vibrations from magnetostriction of the core material to the samples.

Continuous operation with a current of 10 A per DC coil is possible over several minutes without overheating the coils. The generated DC fields inside the air gap attain 600 mT for a gap length of 5 mm and around 190 mT for a gap length of 30 mm in those continuous measurement conditions (see Fig. 4.2). A current of 22 A per coil proved possible for up to one minute of operation, reaching field intensities of 217 mT (30 mm) and a maximum possible field of 910 mT at a gap length of 3 mm - the smallest gap length feasible for measurements.

Simulations showed that the magnetic core material also guides the AC field lines inside the gap, leading to relatively homogeneous AC fields (Fig. 4.4). The core material's influence also leads to large variations in AC field intensities with variations of the gap length (Fig. 4.3 and 4.5).

Measurements of AC field intensities revealed to be relatively constant for frequency variations between 1 and 10 kHz (Fig. 4.3). The slight increase at higher frequencies is probably due to a not yet optimized compensation network of the AC current amplifier, leading to samll variations in current intensities with frequency.

When increasing the DC bias field, the permeability of the core material decreases, leading to decreased superimposed AC field intensities. This effect can be seen in Fig. 4.5.

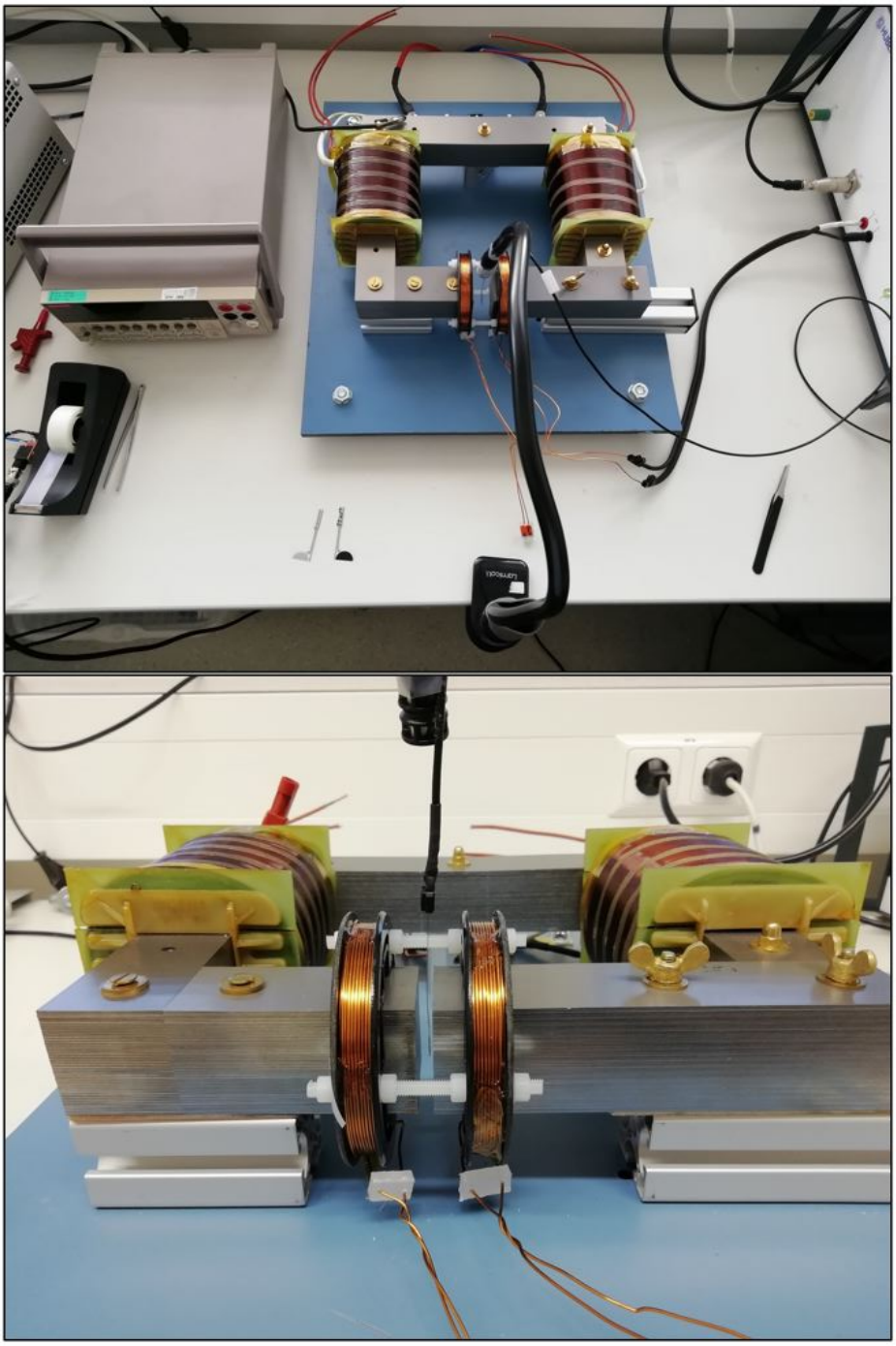

Figure 4.1: Set-up for simultaneous DC and AC magnetic excitation using a core-magnet with an air gap and a Helmholtz-coil-pair for superimposing an AC field. The sample is located free-hanging in the air gap

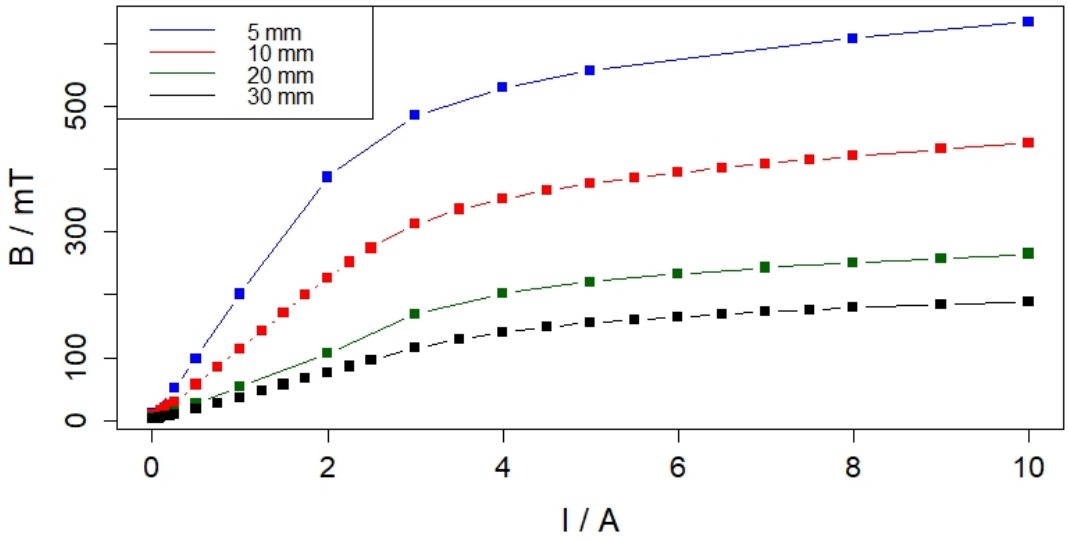

Figure 4.2: Measured DC magnetic field in air gap for different gap lengths vs current per coil

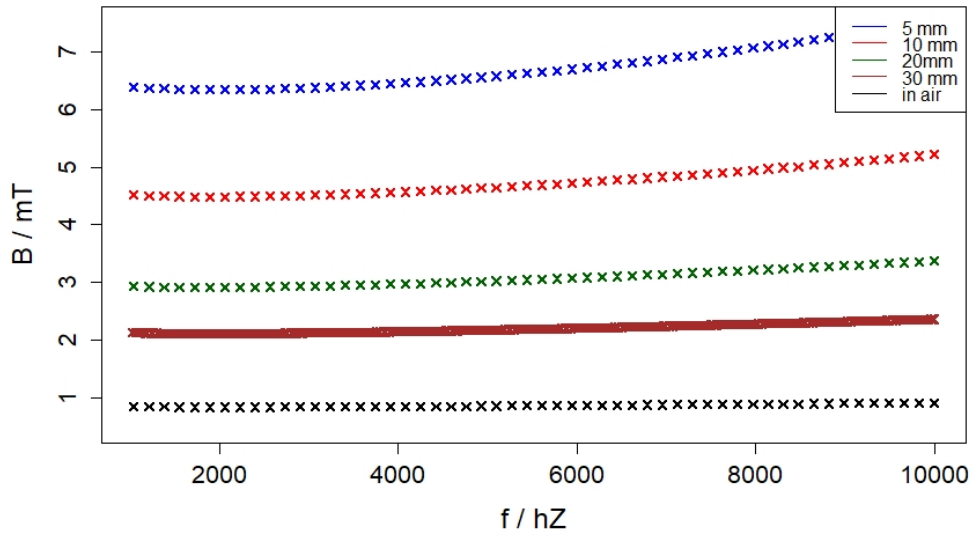

Figure 4.3: Measured AC field vs frequency for different gap lengths and removed from the core ($I_{AC,\,Peak} = 6$ A)

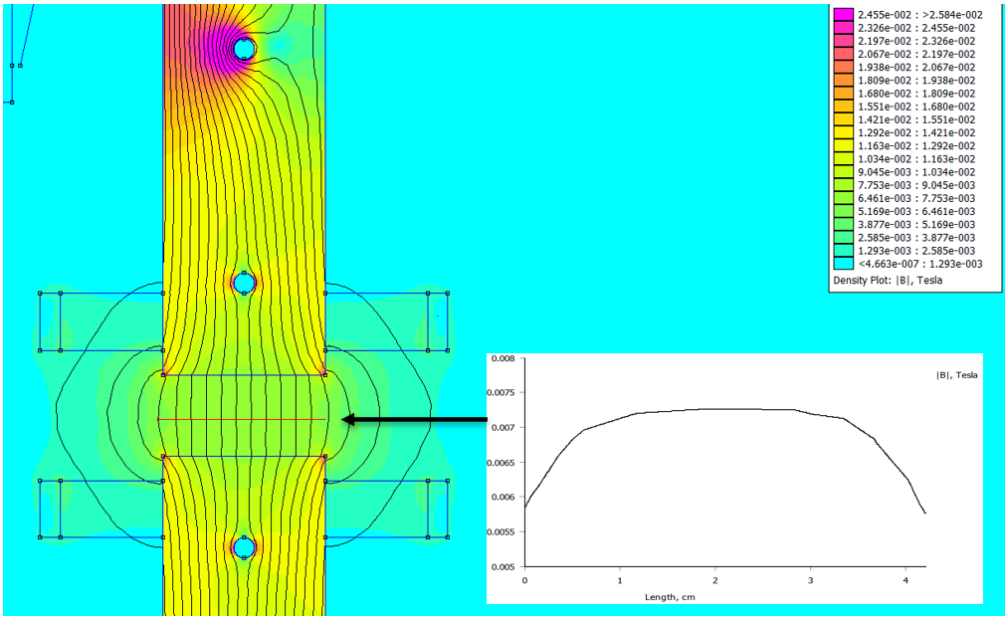

Figure 4.4: Simulation of transverse AC field variations inside an air gap of 20 mm

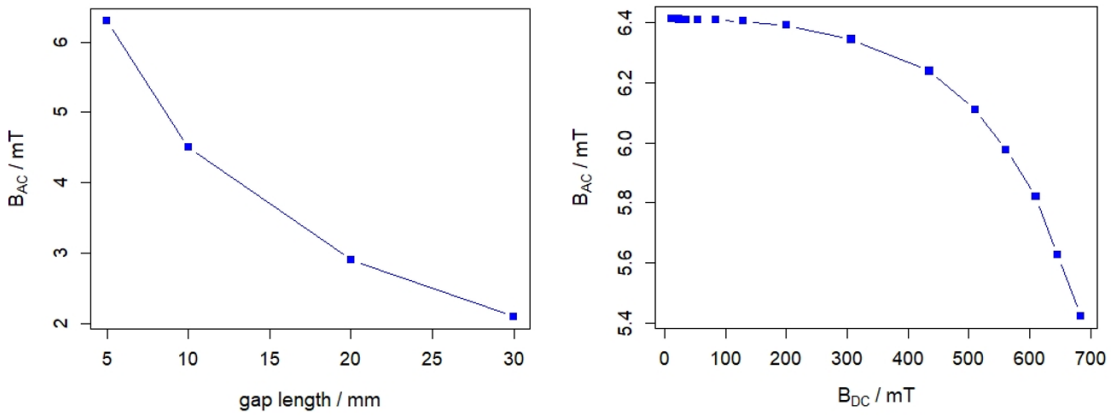

Figure 4.5: AC field vs gap length ($B_{DC} = 0$) and vs DC bias field (gap = 5 mm) - both at $I_{AC,\,Peak} = 6$ A and f = 3.05 kHz

4.2 Composite Inks for Screen Printing

Magnetoelectric nanoparticles were successfully incorporated into a solution of P(VDF/TrFE) (75:25) in GBL. To disperse all clusters, ball milling of the suspension was necessary for a duration of 14 hours. Light microscopy images showed good homogeneity of a dispersion of 50 wt% $CoFe_2O_4$ (relative to P(VDF/TrFE). For testing purposes a dispersion with 70 wt% Fe_3O_4 was created with the same

process, which also showed good homogeneity. Not enough material was available to create a higher wt% dispersion with CFO, but the properties can be expected to be similar to that of FO. The microscopy images are depicted in Fig. 4.6.

The increase in viscosity with the addition of magnetic nanoparticles was compensated with an addition of solvent (GBL).

The highly polar magnetic ionic liquid (bmim[$FeCl_4$) showed perfect miscibility with the polymer solution at 5 and at 24 wt%.

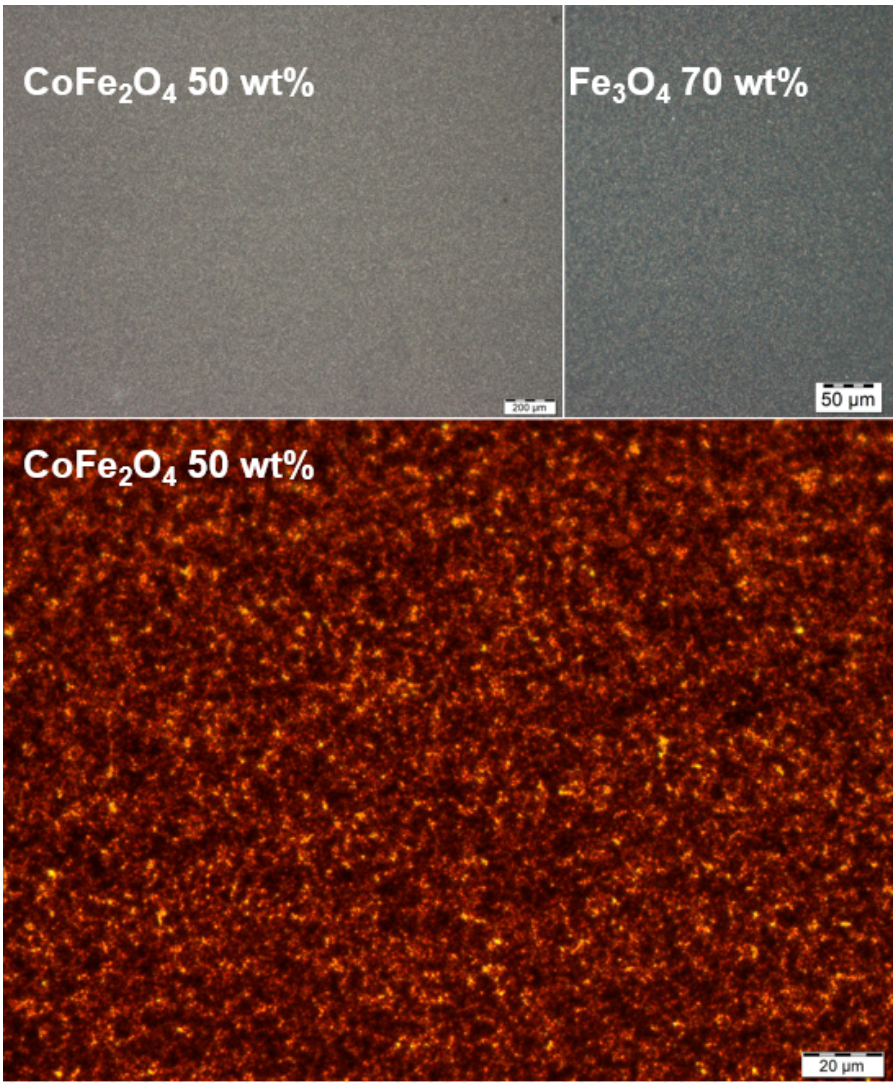

Figure 4.6: Light microscopy images of CFO and FO in a solution of P(VDF/TrFE) in GBL at different magnifications

4.3 Sensor Prototypes

Several magnetoelectric composite sensors were screen printed, filled with 50 wt% CFO and with 5 and 24 wt% MIL, respectively.

A schematic representation of the layered build-up of a round sensor design is given in Fig. 4.7. For measurements this design was cut in the middle and each half was measured individually (see Fig. 4.12).

SEM images showed homogeneous dispersion without large agglomerates of CFO in the 0-3 magnetoelectric phase. The double polymer layer can be destinguished from the composite layer, showing a smooth border between them, while good connectivity between the two stacked phases can be observed (Fig. 4.8).

Fig. 4.9 shows the hysteresis of electric displacement, obtained from the ferroelectric poling process of a sensor made up with the same stacking as in the SEM images in Fig. 4.8. A remnant polarization of 66 mC/m^2 was achieved, with a coercive field of 53 mV/m. This equals a switching field of 844 V between top and botton electrode, where the chains of crystalline β-phase are rotated 180° along their carbon backbone axes. The value for remnant polarization of 66 mC/m^2 is comparable to a reported value of 70 mC/m^2 for a similarly produced ferroelectric P(VDF/TrFE) copolymer without magnetic nanoparticles [32].

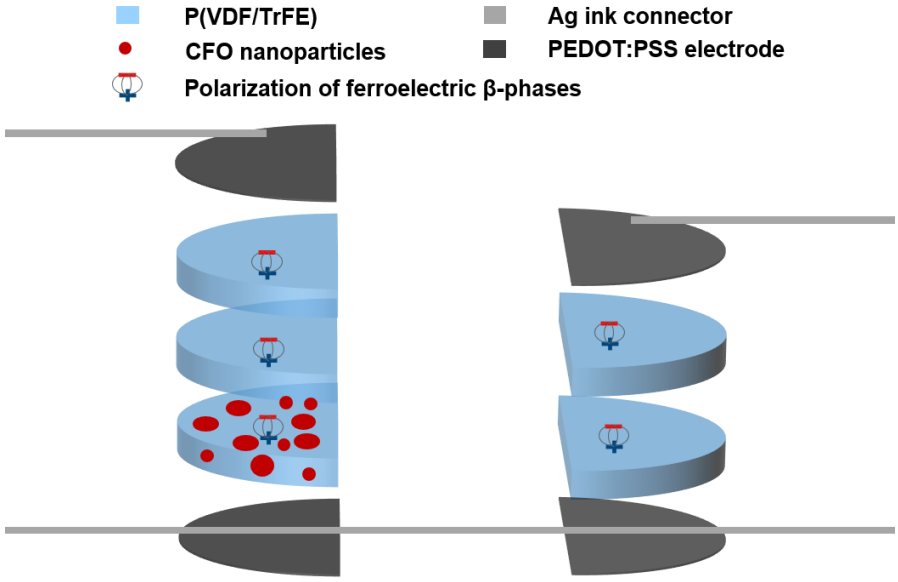

Figure 4.7: Illustration of printed layers of a round sensor design with one magnetoelectric active half and the other half as a piezoelectric reference

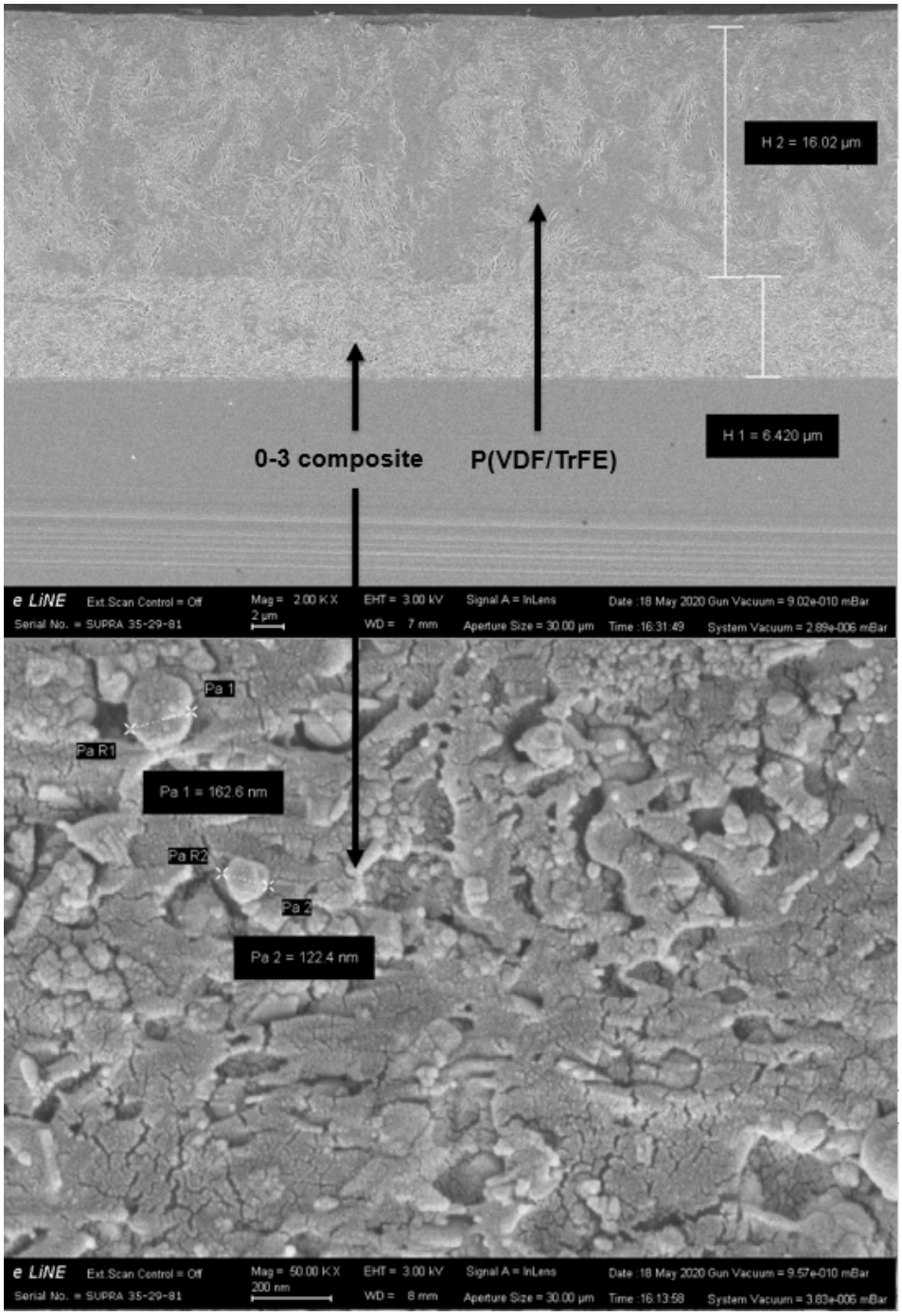

Figure 4.8: SEM image of a microtome cut of a sensor prototype with one screen printed layer of a 50 wt% CFO 0-3 ME composite (bottom panel) and two layers of P(VDF/TrFE) (top panel). Note the different length bars of 2 μm and 200 nm

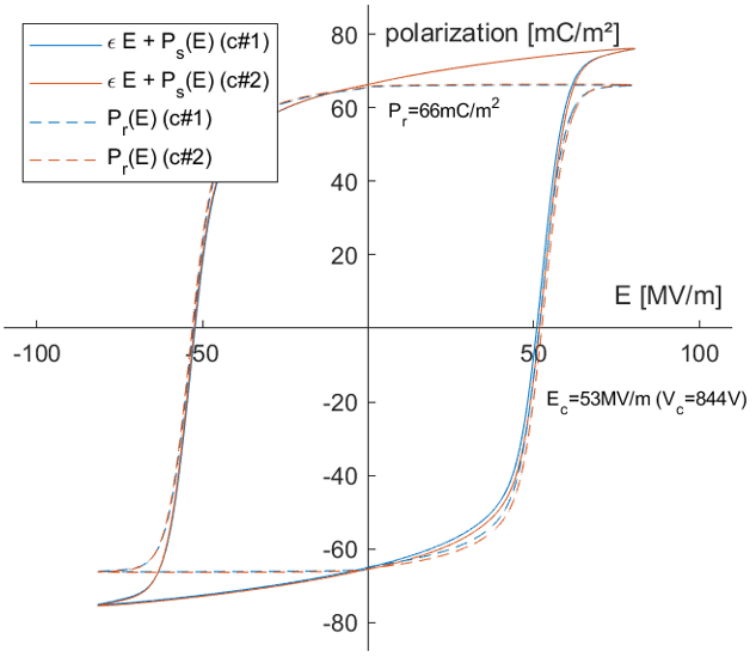

Figure 4.9: Hysteresis curve of electric displacement of the ferroelectric poling process of a sensor with one CFO/P(VDF/TrFE) composite layer and two P(VDF/TrFE) ferroelectric layers. Two cycles (c#1 and c#2) are taken to display the total dielectric polarization (solid line) and after subtraction of the linear field dependent dielectric ploarization (dashed line)

In the sensors produced with 24 wt% MIL, some inclusions, visible as holes, could be observed (Fig. 4.10) but not as many as in the paper cited in 2.5 [11]. The composite solution was screen printed between two layers of pure polymer phase but the inclusions can be seen over all three printed layers. This suggests that the MIL droplets have some mobility within the polymer matrix. Since P(VDF/TrFE) is soluble in polar solvents and the MIL itself is highly polar, it could be able to diffuse through the solid phase. Correia et al. [11] reported no such MIL mobility. Their polymer solution is based on a different solvent (DMF) and higher solvent evaporation temperatures, which could lead to different effects before solvent evaporation.

No droplet inclusions could be observed for the 5 wt% MIL samples (Fig. 4.11).

Analysis of data from magnetoelectric measurements of both MIL samples showed no extractable ME voltage signal. While the concept is very promising, the incorporation of the magnetic ionic liquid into a matrix needs further investigations.

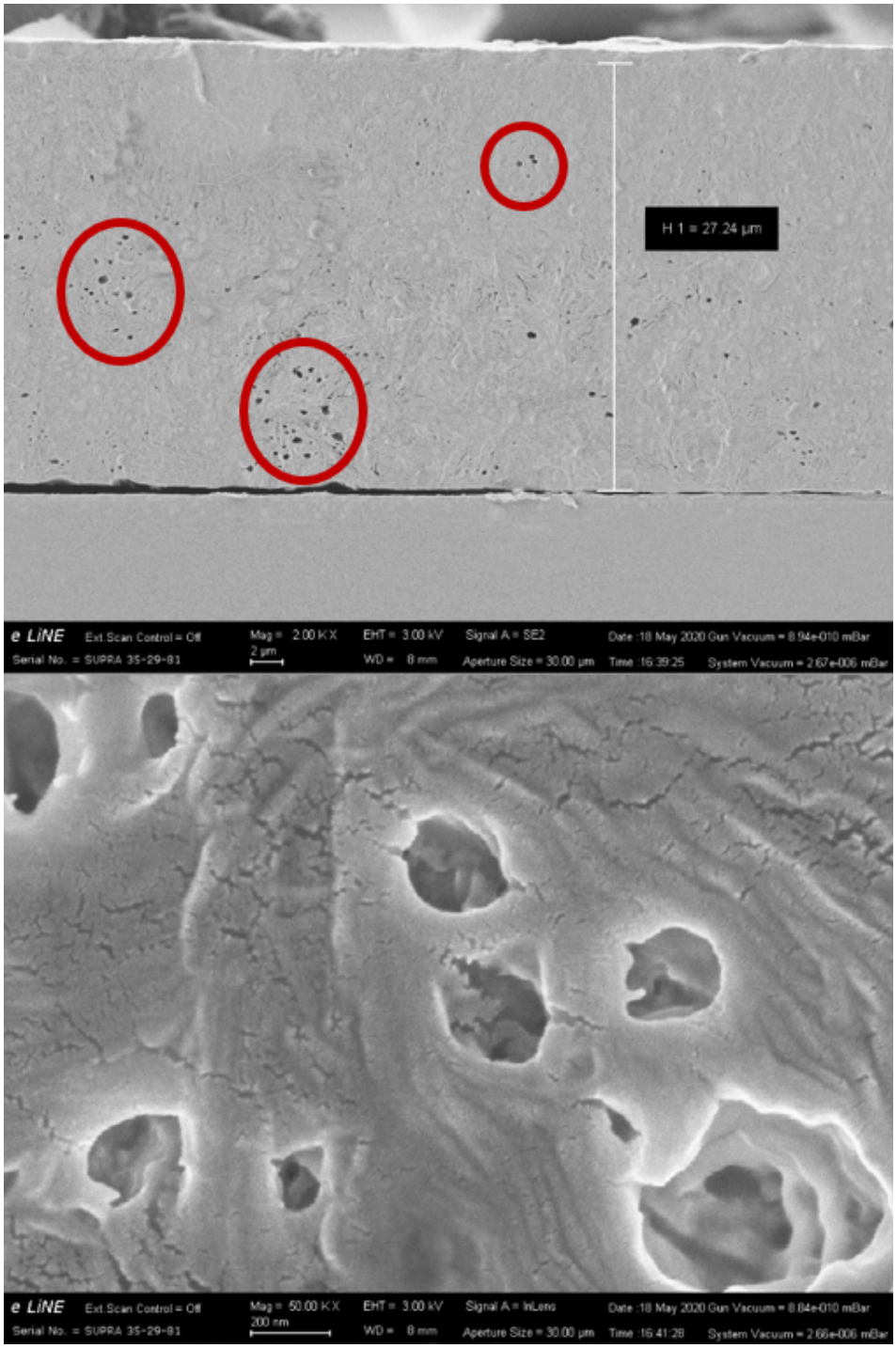

Figure 4.10: SEM images of 24 wt% bmim[$FeCl_4$ in P(VDF/TrFE). Inclusions marked red (top panel) and with higher magnification (bottom panel)

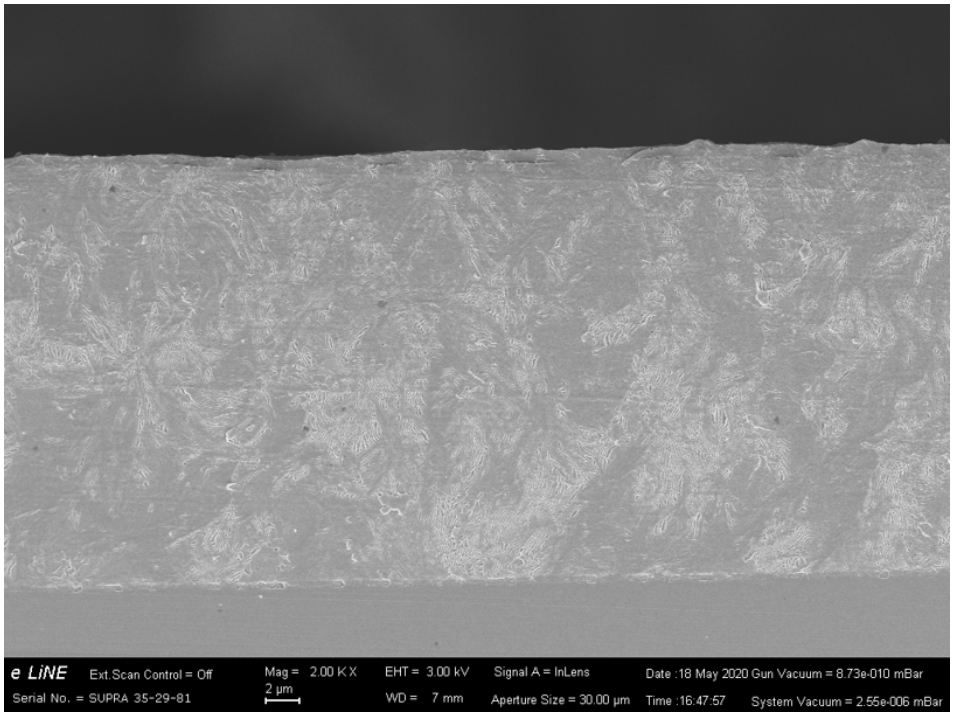

Figure 4.11: SEM image of 5 wt% bmim[$FeCl_4$ in P(VDF/TrFE)

4.4 Measurements

The measurements of the magnetoelectric voltage coefficient showed some unexpected results and large parasitic signals. A quantitative value for α^V could not yet be determined. However, a proof of concept is achieved by measuring a magnetically induced vibration of a composite sensor.

The measurements described in this section were done with the sensor design illustrated in Fig. 4.12 (see also Fig. 4.7). This design has a mirrored axis, with one half being made up of two screen printed layers of P(VDF/TrFE) and the other half being made up of two screen printed layers of P(VDF/TrFE) with an additional screen printed layer of 50 wt% CFO in P(VDF/TrFE). Both halves are sandwiched between two screen printed PEDOT:PSS electrodes. The design was originally intended for compensation measurements. Since bending mode resonant acoustic coupling between both halves is suspected, the sensor was cut in the middle and measurements were taken for each half individually (see Fig. 4.7).

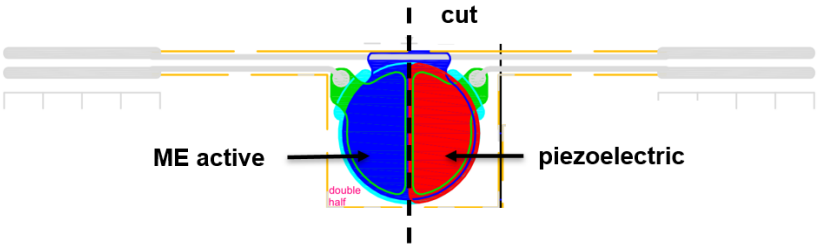

Figure 4.12: Sensor prototype design used in the measurements summarized in this chapter

First, the sample was placed inside a 30 mm air gap of the test bench in an in-plane magnetic field orientation and the piezoelectric phase was excited with a frequency sweep of an AC voltage of 10 V. A laser vibrometer was used to identify mechanical resonance frequencies of the sample. Mechanical resonance could be observed at around 3.05 kHz, which can be seen in Fig. 4.13.

To measure the magnetoelectric output, the gap length was decreased to 5 mm and the sample was placed inside the gap in an out-of-plane orientation, connected to the lock-in amplifier, and a sweep of the magnetic bias field was performed. The DC sweep was performed with a constant superimposed AC magnetic field of 6.5 mT at the suspected resonance frequency of 3.05 kHz. As already stated in 3.5.4, there should be a variation in the ME signal with a sweep of the bias field, while EMF should stay constant, barring small changes in AC field intensity by changes in the magnetic permeability of the test benches' core material.

Fig. 4.14 shows the results of the bias field sweep. As already presented in 3.5.4, an optimal value for the magnetoelectric voltage output would be around 8 $\mathrm{mV_{rms}}$ for this sample. The expected shape of the signal's curve would look like the piezomagnetic coefficient of CFO as a function of magnetic field intensity (see Fig. 2.4 and Fig. 3.8), with almost linear increase until leveling-off at a peak and a subsequent decrease. Since no such signal can be observed, it is reasonable to assume that the magnetoelectric voltage output of the sample is much lower than the maximum expected output.

The lock-in amplifier locks a signal to the reference signal, including phase information, in the form of a phasor of x- and y-components. If an acquired signal has the same phase as the reference signal, it will induce positive values on the x-axis of the acquired signal. A +90 ° phase shifted signal will induce positive values on the y-axis. Often the magnitude of that vector ($Z = (X^2 + Y^2)^{\frac{1}{2}}$) has sufficient information, but Fig. 4.14 shows also the x- and y-components and their

respective variations to emphasize those variations in both signals. This either means that the signal is a mixture of a magnetoelectric signal (expected to have the same phase as the reference signal) and EMF (expected to be 90 ° shifted), or that the lock-in amplifier itself suffers from a phase shift. Similar variations are observed for the ferroelectric reference sample and those variations occur over a wide range of frequencies. With the samples mechanically decoupled from the test bench, the parasitic signals could possibly arise from pressure/sound waves arising from the magnetostriction of the core material in close proximity to the measured sample, but the measurements described later in this work indicate that this is not the case. EMF is still the most likely source of the large parasitic signals, which is surprising, as the AC field's amplitude should stay rather constant over this measurement.

In any case, the parasitic signals are too large and a possible magnetoelectric signal is too small to provide reliable quantitative results at this point.

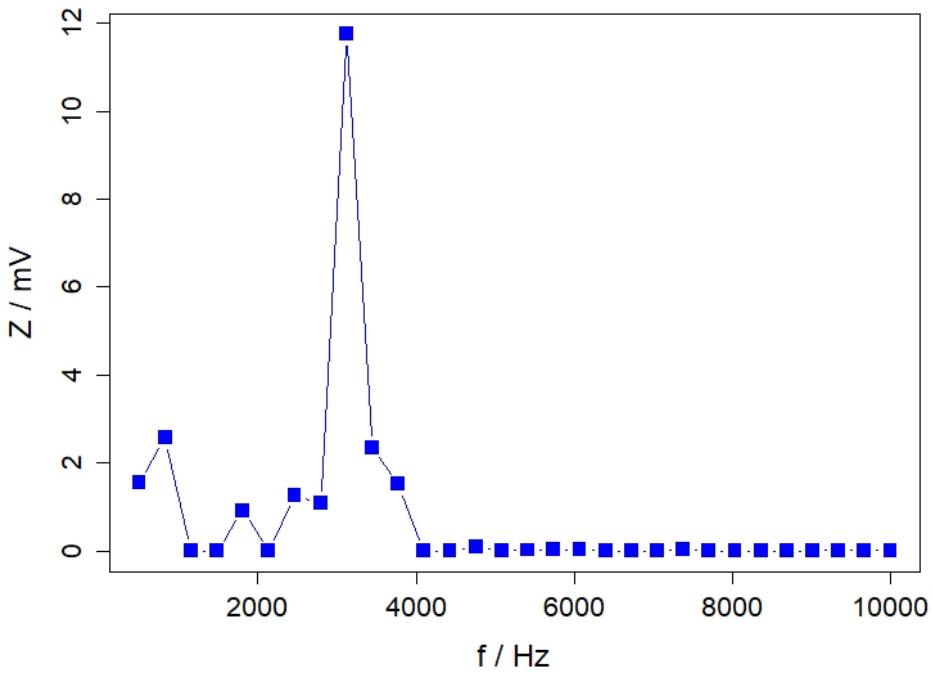

Figure 4.13: Laser vibrometer measurement of the voltage driven magnetoelectric sample

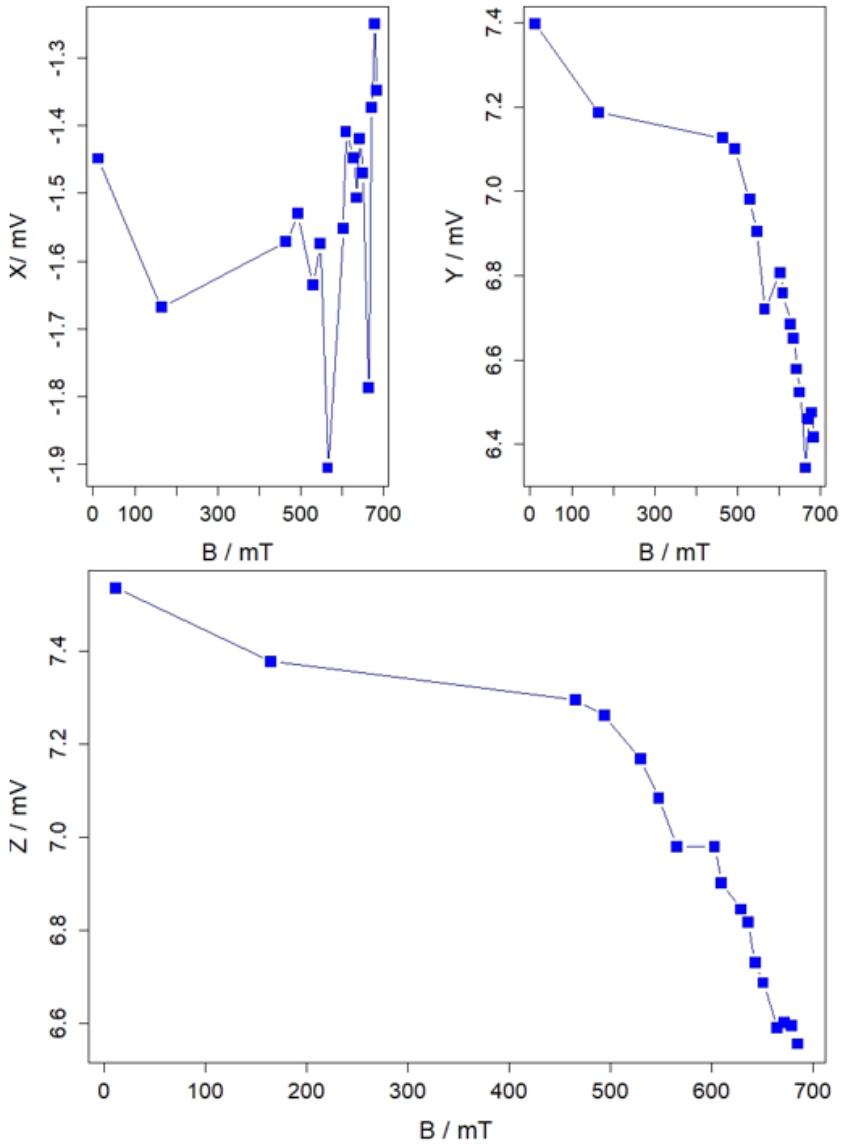

Figure 4.14: Voltage output of the ME sample and connecting lines as guide for the eye vs bias field intensity at f = 3.05 kHz and B_{AC} = 6.5 mT. The upper two panels show the in-phase (=X) and the out-of-phase (=Y) lock-in response, respectively, the lower panel its magnitude (=Z) response

Ensuring a measurement without any parasitic signals arising from EMF, laser vibrometer measurements were taken of both the magnetoelectric and the reference sample. At predetermined resonance frequencies, each sample was first driven by voltage, exciting the ferroelectric phase, and then by an AC magnetic field, ex-

pecting bending vibrations from electro- and magnetostriction, respectively. The samples were placed in the 30 mm air gap in an in-plane orientation and were not moved between the two measurements.

It can be seen from Fig. 4.15 and Fig. 4.16 that both samples gave a rather large response when they were electrically excited (upper panels), but only the magnetoelectric sample responded upon magnetic excitation (lower panel of Fig. 4.15). The missing data points in the magnetically excited measurement of the reference sample (lower panel of Fig. 4.16) come from the fact that the lock-in amplifier, connected to the vibrometer, could not be phase-locked to any signal in the frequency range of 3070 - 3170 Hz. This measurement was repeated several times without any success of phase-locking.

A possible false signal from a direct magnetic force on the particles themselves is possible but unlikely, since the mass of cobalt ferrite in the sample is below 500 μg and the magnetic field is relatively weak at 2.1 mT.

Those measurements can be interpreted to lead to two conclusions. First, a magneto-electric signal is present, and either the measurement set-up needs to be improved, or the samples' output needs to be increased to get quantitative measurements. Second, the samples are sufficiently decoupled from the test bench and a transfer of vibrations from the test bench core material through sound or pressure waves is not giving large parasitic signals.

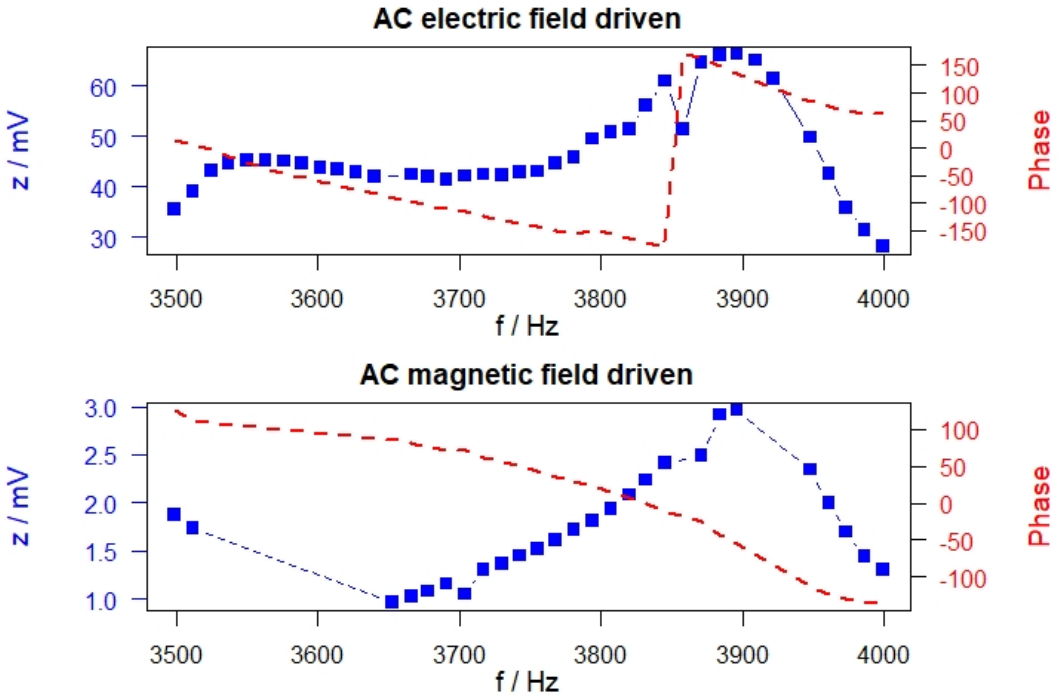

Figure 4.15: Laser vibrometer measurements of the magnetoelectric sample. Z = magnitude response (blue symbols), and phase-response (dashed red lines).
Top: voltage driven (10 V)
Bottom: driven by B_{AC} (2.1 mT)

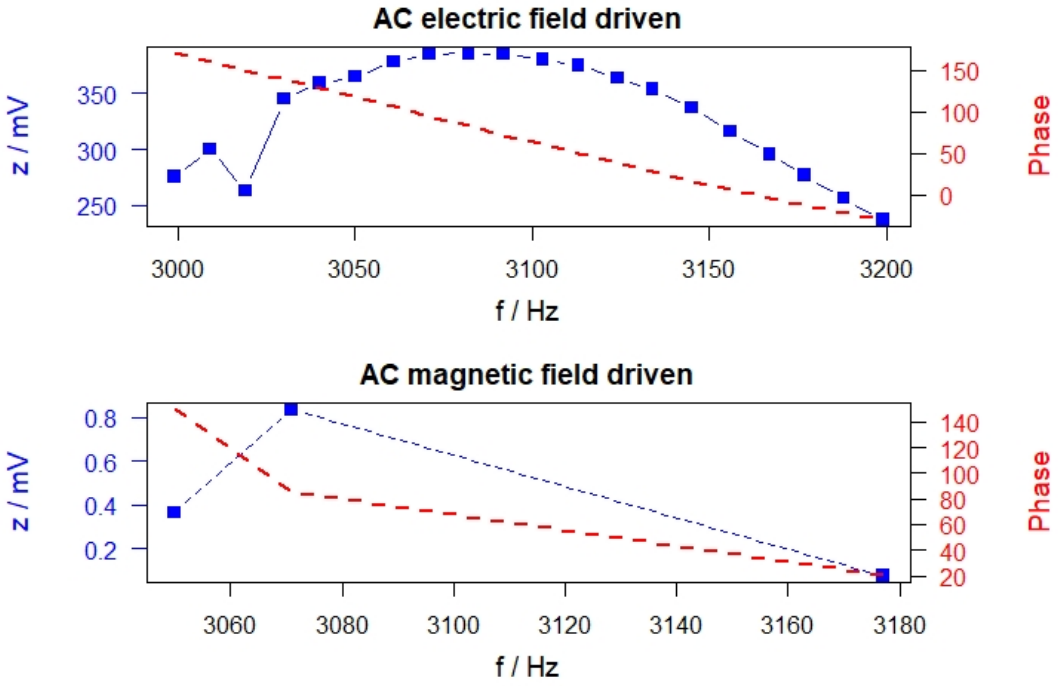

Figure 4.16: Laser vibrometer measurements of the ferroelectric reference sample (without magnetic entities). Z = magnitude response (blue symbols), and phase-response (dashed red lines). Note: magnetic excitation (lower panel) cannot excite any acoustic resonance. The dashed blue line represents noisy data which is not plotted.
Top: voltage driven (10 V)
Bottom: driven by B_{AC} (2.1 mT)

5 Conclusion

It has been shown that the dedicated concept of the sensor design with magnetostrictive nanoparticles works as intended if electric and acoustic noise is cancelled by proper compensation. Therefore, a lot of effort has been put into a possible suppression of parasitic signals and further improvements may not be achieved easily. At the state-of-the-art, the ME effect in 0-3 and 2-2 connected magnetoelectric polymer foils has been proven successfully by detecting magnetostrictive resonances using laser vibrometry, but an electric quantification of the ME effect is still lacking. With the need for improving the ratio of magnetoelectric and parasitic signal to reliably extract a low-level magnetoelectric signal in polymer-based ME sensors, the sensitivity has to be increased. Especially with the intention of creating sensors that might be used to sense minute variations of magnetic field intensities, a significant increase in the sensors' output is needed.

Unfortunately a proper development of the sensor concept using magnetic ionic liquids failed within the scope of this thesis work. Nonetheless, the first trials we did are promising and they were still included, since the concept has such high potential. The publications on which we base our access to this problem are promising: magnetic ionic liquids could radically improve the applicability of magnetoelectric composite sensors. Production could be possible without any ressource-intensive processes and without any high-cost materials, possibly leading to cheap mass production of sensors. Further investigations are definitely necessary.

6 Outlook

Several routes for improving the sensors' magnetoelectric voltage output are possible.

With the ME voltage signal linearly depending on composite thickness, the most simple way for improvements would be to increase the sample's thickness by printing several stacks on top of each other. The 0-3 composite layers in the samples investigated in this work have thicknesses of little more than 5 μm, while the work of Lima et al. [9], which our work is partly based on, uses layers with a thickness of around 100 μm. We can generate larger AC fields than they do, but with increasing the intensity of the time-varying magnetic field, the parasitic signals increase as well.

A problem we had was that we could only create a sample with 50 wt% CFO because we did not have more cobalt ferrite available, while Lima's group used 85 wt% CFO. The output should not increase linearly and should be more than a factor of 1.7 (=85/50) times higher at 85 wt%. This concentration definitely needs to be maximized. It was shown in this work that a 70 wt% Fe_3O_4 ink could be produced for our screen printing process - at least that concentration should also be possible for $CoFe_2O_4$.

Another way to increase the ME output would be to use materials with a higher piezomagnetic coefficient. Two very promising candidates are presented in Fig. 6.1. Titanium substituted cobalt ferrite and samarium substituted nickel ferrite both show a large increase in piezomagnetic coefficients compared to their unsubstituted form [34] [41]. The lower panel of Fig. 6.1 a) is a plot of the strain derivative with respect to the magnetic field (piezomagnetic coefficient) of titanium substituted CFO (blue curve) in comparison with CFO (red curve), showing a substantially higher peak for the Ti substituted material. From the curves of Fig. 6.1 b) it can be seen that samarium substituted nickel ferrite ($NiFe_{1.925}Sm_{0.075}O_4$ - red star markers) reaches a magnetostriction of -15 ppm at a field intensity of around 0.2 kOe while nickel ferrite (blue markers) reaches similar magnetostriction values at around 0.8 kOe. This indicates a fourfold increase in piezomagnetic coefficient at very low field intensities.

The magneto ionic liquid route is very promising and should be investigated along with other options. The liquid can be encapsulated in any dielectric material and further investigation could prove very fruitful.

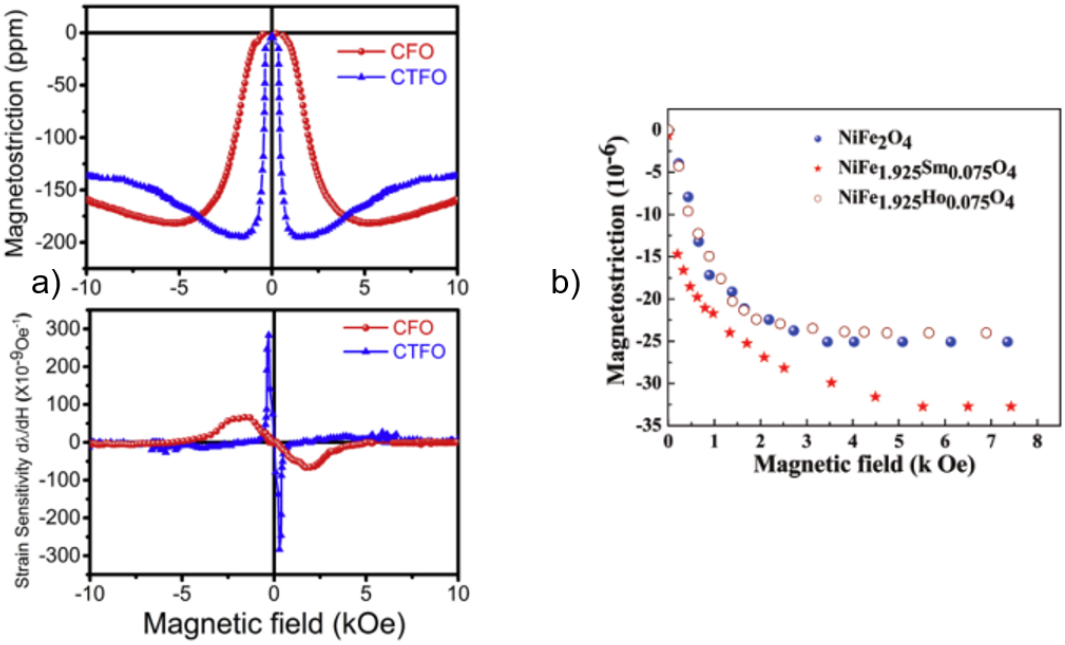

Figure 6.1: Enhanced piezomagnetic coefficient in a) Ti substituted $CoFe_2O_4$ [34] and b) Sm substituted $NiFe_2O_4$ [41]

References

[1] N. A. Spaldin and R. Ramesh. Advances in magnetoelectric multiferroics. *Nature Materials*, 18(3):203–212, February 2019.

[2] C M Leung, J Li, D Viehland, and X Zhuang. A review on applications of magnetoelectric composites: from heterostructural uncooled magnetic sensors, energy harvesters to highly efficient power converters. *Journal of Physics D: Applied Physics*, 51(26):263002, June 2018.

[3] Y Cheng, B Peng, Z Hu, Z Zhou, and M Liu. Recent development and status of magnetoelectric materials and devices. *Physics Letters A*, 382(41):3018–3025, October 2018.

[4] Z Chu, M Javad, P Asl, and S Dong. Review of multi-layered magnetoelectric composite materials and devices applications. *Journal of Physics D: Applied Physics*, 51(24):243001, May 2018.

[5] H Palneedi, V Annapureddy, S Priya, and J Ryu. Status and perspectives of multiferroic magnetoelectric composite materials and applications. *Actuators*, 5(1):9, March 2016.

[6] M. M. Vopson, Y. K. Fetisov, G. Caruntu, and G. Srinivasan. Measurement techniques of the magneto-electric coupling in multiferroics. *Materials*, 10(8):963, August 2017.

[7] J Ryu, S Priya, K Uchino, and H Kim. Magnetoelectric effect in composites of magnetostrictive and piezoelectric materials. *Journal of Electroceramics*, 8(2):107–119, 2002.

[8] P. Martins, Yu. V. Kolen'ko, J. Rivas, and S. Lanceros-Mendez. Tailored magnetic and magnetoelectric responses of polymer-based composites. *ACS Applied Materials & Interfaces*, 7(27):15017–15022, July 2015.

[9] A. C. Lima, N. Pereira, R. Policia, C. Ribeiro, V. Correia, S. Lanceros-Mendez, and P. Martins. All-printed multilayer materials with improved magnetoelectric response. *Journal of Materials Chemistry C*, 7(18):5394–5400, 2019.

[10] P Lanceros-Méndez, S; Martins. *Magnetoelectric polymer-based composites : fundamentals and applications*. Wiley VCH, 2017.

[11] D. M. Correia, P. Martins, M. Tariq, J. M. S. S. Esperança, and S. Lanceros-Méndez. Low-field giant magneto-ionic response in polymer-based nanocomposites. *Nanoscale*, 10(33):15747–15754, 2018.

[12] W. C. Röntgen. Ueber die durch bewegung eines im homogenen electrischen felde befindlichen dielectricums hervorgerufene electrodynamische kraft. *Annalen der Physik und Chemie*, 271(10):264–270, 1888.

[13] P. Debye. Bemerkung zu einigen neuen versuchen über einen magneto-elektrischen richteffekt. *Zeitschrift für Physik*, 36(4):300–301, April 1926.

[14] D. N. Astrov. The magnetoelectric effect in antiferromagnetics. *Soviet Physics JETP*, 11(3), 1960.

[15] I.E. Dzyaloshinskii. The magnetoelectric effect in antiferromagnetics. *Soviet Physics JETP*, 10(3), 1959.

[16] W. F. Brown, R. M. Hornreich, and S. Shtrikman. Upper bound on the magnetoelectric susceptibility. *Physical Review*, 168(2):574–577, April 1968.

[17] T Sano (eds.) C Kim, C Randow. *Hybrid and Hierarchical Composite Materials*. Springer International Publishing, 1 edition, 2015.

[18] J. X. Zhang, J. Y. Dai, L. C. So, C. L. Sun, C. Y. Lo, S. W. Or, and H. L. W. Chan. The effect of magnetic nanoparticles on the morphology, ferroelectric, and magnetoelectric behaviors of CFO/p(VDF-TrFE) 0–3 nanocomposites. *Journal of Applied Physics*, 105(5):054102, March 2009.

[19] P Martins, X Moya, L C Phillips, S Kar-Narayan, N D Mathur, and S Lanceros-Mendez. Linear anhysteretic direct magnetoelectric effect in ni0.5zn0.5fe2o4/poly(vinylidene fluoride-trifluoroethylene) 0-3 nanocomposites. *Journal of Physics D: Applied Physics*, 44(48):482001, November 2011.

[20] P. Martins, X. Moya, C. Caparrós, J. Fernandez, N. D. Mathur, and S. Lanceros-Mendez. Large linear anhysteretic magnetoelectric voltage coefficients in CoFe2o4/polyvinylidene fluoride 0–3 nanocomposites. *Journal of Nanoparticle Research*, 15(8), July 2013.

[21] J. Zhai, J. Li, D. Viehland, and M. I. Bichurin. Large magnetoelectric susceptibility: The fundamental property of piezoelectric and magnetostrictive laminated composites. *Journal of Applied Physics*, 101(1):014102, January 2007.

[22] G Wu, T Nan, R Zhang, N Zhang, S Li, and N X Sun. Inequivalence of direct and converse magnetoelectric coupling at electromechanical resonance. *Applied Physics Letters*, 103(18):182905, October 2013.

[23] J. van Suchtelen. Product properties: A new application of composite materials. *Philips Research Reports*, 27:28–37, 1972.

[24] M. I. Bichurin, V. M. Petrov, and G. Srinivasan. Theory of low-frequency magnetoelectric coupling in magnetostrictive-piezoelectric bilayers. *Physical Review B*, 68(5), August 2003.

[25] M. I. Bichurin, V. M. Petrov, S. V. Averkin, and A. V. Filippov. Electromechanical resonance in magnetoelectric layered structures. *Physics of the Solid State*, 52(10):2116–2122, October 2010.

[26] M. I. Bichurin, V. M. Petrov, S. V. Averkin, and E. Liverts. Present status of theoretical modeling the magnetoelectric effect in magnetostrictive-piezoelectric nanostructures. part i: Low frequency and electromechanical resonance ranges. *Journal of Applied Physics*, 107(5):053904, March 2010.

[27] M. I. Bichurin, V. M. Petrov, S. V. Averkin, and E. Liverts. Present status of theoretical modeling the magnetoelectric effect in magnetostrictive-piezoelectric nanostructures. part II: Magnetic and magnetoacoustic resonance ranges. *Journal of Applied Physics*, 107(5):053905, March 2010.

[28] Vladimir Petrov Mirza Bichurin. *Modeling of Magnetoelectric Effects in Composites*. Springer Series in Materials Science 201. Springer Netherlands, 1 edition, 2014.

[29] Martins P.; Lopes A.C.; Lanceros-Mendez S. Electroactive phases of poly(vinylidene fluoride): Determination, processing and applications. *Progress in Polymer Science*, 39, 04 2014.

[30] Zirkl M. *Herstellung und Charakterisierung von ferroelektrischen Polymer-Dünnfilmen und ihre Anwendung in integrierten organischen Infrarotsensoren.* Karl-Franzens Universität Graz, Dissertation, 2007.

[31] B Stadlober, M Zirkl, and M Irimia-Vladu. Route towards sustainable smart sensors: ferroelectric polyvinylidene fluoride-based materials and their integration in flexible electronics. *Chemical Society Reviews*, 2019.

[32] M Zirkl, G Scheipl, B Stadlober, C Rendl, P Greindl, M Haller, and P Hartmann. Pyzo flex®: A printed piezoelectric pressure sensing foil for human machine interfaces. *Proceedings of SPIE - The International Society for Optical Engineering*, 8831, 09 2013.

[33] I. C. Nlebedim, J. E. Snyder, A. J. Moses, and D. C. Jiles. Anisotropy and magnetostriction in non-stoichiometric cobalt ferrite. *IEEE Transactions on Magnetics*, 48(11):3084–3087, November 2012.

[34] J. P. Praveen, V. R. Monaji, E. Chandrakala, S. Indla, S. D. Kumar, V. Subramanian, and D. Das. Enhanced magnetoelectric coupling in ti and ce substituted lead free CFO-BCZT laminate composites. *Journal of Alloys and Compounds*, 750:392–400, June 2018.

[35] Carmen-Gabriela Stefanita (auth.). *Magnetism: Basics and Applications*. Springer-Verlag Berlin Heidelberg, 1 edition, 2012.

[36] D. R. MacFarlane, M. Kar, and J. M. Pringle. *Fundamentals of ionic liquids*. Wiley-VCH, 2017.

[37] K Bica, M Deetlefs, C Schröder, and K R Seddon. Polarisabilities of alkylimidazolium ionic liquids. *Physical Chemistry Chemical Physics*, 15(8):2703, 2013.

[38] Birgit Weber. *Koordinationschemie: Grundlagen und aktuelle Trends*. Springer Spektrum, 1 edition, 2014.

[39] Kumidas SA. *Safety Data Sheet KUMIoF212*. 2019.

[40] D. Meeker. *Finite Element Method Magnetics Version 4.2 User's Manual*, 2018.

[41] B. K. Kamala, M. G., and C. V Ramana. Structural, magnetic, electrical, and magnetoelectric properties of sm- and ho-substituted nickel ferrites. *The Journal of Physical Chemistry C*, 115, 2011.